HHS Public Access

Author manuscript

Nat Chem Biol. Author manuscript; available in PMC 2025 September 01.

Published in final edited form as:

Nat Chem Biol. 2025 March ; 21(3): 360–370. doi:10.1038/s41589-024-01705-2.

An engineered trafficking biosensor reveals a role for DNAJC13 in DOR downregulation

Brandon Novy[1], **Aleksandra Dagunts**[1], **Tatum Weishaar**[1], **Emily E. Holland**[1], **Hayden Adoff**[1], **Emily Hutchinson**[1], **Monica De Maria**[1], **Martin Kampmann**[2], **Nikoleta G. Tsvetanova**[3], **Braden T. Lobingier**[1,#]

[1]Department of Chemical Physiology and Biochemistry, Oregon Health & Science University, Portland, OR

[2]Department of Biochemistry and Biophysics and Institute for Neurodegenerative Disease, University of California, San Francisco, San Francisco, CA

[3]Department of Pharmacology and Cancer Biology, Duke University, Durham, NC

Abstract

Trafficking of G protein-coupled receptors (GPCRs) through the endosomal-lysosomal pathway is critical to homeostatic regulation of GPCRs following activation with agonist. Identifying the genes involved in GPCR trafficking is challenging due to the complexity of sorting operations and the large number of cellular proteins involved in the process. Here, we developed a high-sensitivity biosensor for GPCR expression and agonist-induced trafficking to the lysosome by leveraging the ability of the engineered enzyme APEX2 to activate the fluorogenic substrate Amplex UltraRed (AUR). We used the GPCR-APEX2/AUR assay to perform a genome-wide CRISPR interference screen focused on identifying genes regulating expression and trafficking of the delta opioid receptor (DOR). We identified 492 genes consisting of both known and novel regulators of DOR function. We demonstrate that one novel regulator, DNAJC13, controls trafficking of multiple GPCRs, including DOR, through the endosomal-lysosomal pathway by regulating the composition of the endosomal proteome and endosomal homeostasis.

corresponding author.

Author Contributions

BTL conceived and directed the study. BN, BTL, AD, EEH performed APEX2/AUR assays. BTL, BN, EH, and ED performed western blots. BN and BTL performed imaging experiments. BN, BTL, TW , and AD performed flow cytometry. Constructs were cloned by EEH, BN, and BTL. CRISPRi assays were performed by BN, MdM, and BTL. Nociceptor data analysis was performed by HA. Imaris rendering performed by BN. Adjacency scoring performed by HA. Endosome diameter measured by BTL. BN and HA performed APEX proximity labeling and proteomic sample preparation. BTL and BN prepared the figures. BTL wrote the manuscript with critical feedback from other coauthors.

Competing Interests

M.K. is a co-scientific founder of Montara Therapeutics and serves on the Scientific Advisory Boards of Engine Biosciences, Casma Therapeutics, Cajal Neuroscience, Alector, and Montara Therapeutics, and is an advisor to Modulo Bio and Recursion Therapeutics. M.K. is an inventor on US Patent 11,254,933 related to CRISPRi and CRISPRa screening, and on a US Patent application on *in vivo* screening methods. The remaining authors declare no other competing interests with the content of this article.

Contact for Reagent and Resource Sharing

Requests for resources, reagents, or further information about methods should be directed to Lead Contact Braden Lobingier (lobingib@ohsu.edu)

Introduction

G protein-coupled receptors (GPCRs) modulate the physiological responses to many hormones and neurotransmitters. GPCR trafficking is a key part of the homeostatic response which regulates receptors at the cellular level following agonist binding.[1] GPCRs can undergo agonist-stimulated endocytosis followed by sorting at endosomes into pathways that either lead back to the cell surface or to the lysosome.[1] While trafficking back to the cell surface is linked to resensitization of cellular signaling potential, trafficking of receptors to the lysosome leads to proteolysis of the receptor, downregulation of agonist binding sites, and subsequent loss of cellular responsiveness to agonists.[2] A fundamental challenge has been to identify the proteins which mediate trafficking of GPCRs through the endosomal-lysosomal pathway and thus control receptor function following agonist binding.

We reasoned that genetics would be a powerful approach to identify cellular proteins which regulate receptor movement through the endosomal-lysosomal pathway, capturing both direct interacting proteins as well as proteins which control specific steps in the pathway. CRISPR-based techniques have revolutionized mammalian genetics, and pooled genetic screens have made it tractable to interrogate the entire mammalian genome.[3] One challenge to the pooled genetic screen approach is that it requires a phenotype-responsive assay with a large dynamic range, and many pooled screens use fluorescence activated cell sorting (FACS) to identify sgRNAs which affect the phenotype of interest.[4] Classical methods for looking at agonist-induced GPCR trafficking to the lysosome, including western blot, radioligand binding, or co-localization of GFP with lysosomal makers, each have strengths but assay-specific limitations for use in a pooled genetic screen.[5–7] We wanted to combine the strengths of these approaches by developing a high-throughput, sortable, and highly sensitive assay that could be used in pooled genetic screens to capture genes involved in GPCR trafficking through the endosomal-lysosomal pathway. We hypothesized that the engineered enzyme APEX2 could fit these requirements.

APEX2 is an engineered peroxidase that can oxidize different substrates including fluorogenic molecules like Amplex Ultra Red (AUR).[8] APEX2 can amplify signal through multiple substrate turnover events and, as it was derived from a cytoplasmic protein, we reasoned its activity would be rapidly quenched by proteases and the low pH in the lysosome. Thus, our approach here was to test if APEX2, as a genetic fusion to a GPCR (GPCR-APEX2), could function as a biosensor for GPCR expression and downregulation resulting from trafficking to the lysosome. In the GPCR-APEX2 construct design, APEX2 co-traffics with GPCR and resides in the cytoplasm until involution into late endosomal multi-vesicular bodies (MVBs) and delivery to lysosome. An additional advantage of using an APEX2-based biosensor is that we and others have recently shown that APEX2 can mediate high-resolution proximity labeling by oxidizing biotin-phenol (BP).[9–11] Thus, we considered that our GPCR-APEX2/AUR method could potentially be combined with GPCR-APEX2/BP to create a single platform for genomic and proteomic interrogating of GPCR trafficking.

We selected the delta opioid receptor (DOR) as the GPCR to test our chemical biology method. On the physiological level, the DOR modulates anxiety and pain.[12,13] On

the cellular level, the DOR is a prototypical example of a GPCR which undergoes agonist-dependent endocytosis followed by efficient trafficking to the lysosome for downregulation.[13] The lifecycle of DOR trafficking starts in the secretory pathway where known interactions with the COPI coatomer complex regulate its movement to the cell surface.[14,15] At the plasma membrane, high efficacy agonists stimulate DOR signaling and DOR phosphorylation by GPCR kinases.[16] β-arrestin binds phosphorylated DOR and recruits it to clathrin-coated pits for endocytosis.[16]At the endosome a few genes have been identified in controlling DOR trafficking to the lysosome including GASP-1, E3 ubiquitin ligases, and ubiquitin binding proteins.[6,9,17] However, these proteins only represent a partial view of what is required to traffic DOR and other GPCRs through the endosomal-lysosomal pathway.[2,13] Here, we sought to fill in the gaps in our understanding of GPCR trafficking by creating a genetic map in human cells of the genes required for DOR expression and downregulation resulting from agonist-stimulated trafficking to the lysosome.

Results

APEX2-based fluorescence biosensor for GPCR downregulation

We first examined if tagging the DOR with APEX2 disrupted receptor function. Consistent with previous studies showing the DOR is amenable to C-terminal tagging, we found that the APEX2 tag had no measurable effects on DOR signaling, agonist-induced degradation, or sub-cellular localization and caused a small increase (2.7 %) in agonist-induced endocytosis (Extended Data Fig. 1A–F).[9,18] Together, these data demonstrate that the APEX2 tag is tolerated by the DOR. We next sought to characterize the ability of the GPCR-APEX2/AUR reaction to detect GPCR expression. We first tested its sensitivity and linear range using defined numbers of HEK293 cells stably expressing DOR-APEX2 without agonist stimulation. We found that the APEX2/AUR assay had a signal-to-noise >500-fold, over two logs of linear range, and its brightness could be readily tuned by changing the amount of AUR in the reaction (Extended Data Fig. 2A–B). We next wanted to compare the GPCR-APEX2/AUR to a field-standard approach for detecting expression, GFP-tagging. We created a new construct, DOR-APEX2-GFP, to compare these approaches directly and found that the GPCR-APEX2/AUR had 200-fold greater signal-to-noise compared to GFP (Extended Data Fig. 2C). Together, these results demonstrate that the GPCR-APEX2/AUR assay is a highly sensitive and tunable method for detecting GPCR expression.

We next asked if APEX2 activity would be quenched by agonist-induced trafficking of the DOR to the lysosome (Fig. 1A). To do this, we developed the lysate version APEX2/AUR assay in which cellular membranes were rapidly permeabilized with TritonX-100, reacted for 1-minute reaction with AUR and hydrogen peroxide, and quenced with 100-fold molar excess of the competitive substrate sodium L-ascorbate. We stimulated HEK293 cells stably expressing DOR-APEX2 with the specific DOR agonist DADLE for different times before performing the APEX2/AUR reaction. We found the signal was indeed lost upon agonist treatment with kinetics consistent to the known rates of DOR trafficking the lysosome (Fig. 1B).[6,7] To verify that the loss of the APEX2/AUR fluorescent reaction was due to agonist-dependent trafficking of the DOR-APEX2, we performed a competition experiment in which increasing amounts of the DOR antagonist naloxone were added together with the

agonist DADLE. We found that the antagonist naloxone could block agonist-induced loss of signal in the APEX2/AUR reaction (Fig. 1C). Consistent with signal loss coming from trafficking of the DOR-APEX2 to the lysosome, pre-incubation with the lysosomotropic compound chloroquine, which increases endosomal-lysosomal pH and decreases activity of lysosomal proteases, strongly blunted the agonist-induced loss of APEX2 activity (Fig. 1D).

To adapt the APEX2/AUR assay for single cell sorting, we developed a version for intact cells by applying a transient pulse of sodium azide to quench the reaction and bovine serum albumin to scavenge excess dye.[19] We characterized the reaction product of the APEX2/AUR assay, Amplex Ultrox Red (AUxR), for use in FACS and observed robust signal in multiple channels, with the APC channel (Ex: 633 nm; Filter: 670/30 nm) providing the best signal-to-noise (Extended Data Fig. 2D). We next examined the stability of AUxR in cells, which we reasoned would be trapped in cells due in its non-protonated, fluorescent state pKa (~4).[20,21] We observed the reaction product excited by the 633 nm laser (APC channel) to be stably deposited in cells, and we used this condition for all our intact cell experiments and genetic screening (Extended Data Fig. 2E). During this characterization we noticed signal excited by the blue laser (GFP channel: Ex: 488 nm; Filter: 575/25 nm) showed less stability over time (Extended Data Fig. 2E). While further studies will be necessary to define the basis of this differential behavior, studies of a highly similar reaction (oxidation of Amplex Red by horse radish peroxidase) noted the potential for multiple reaction products.[21] We next wanted to validate the intact version of the APEX2/AUR assay for DOR trafficking to the lysosome. As in the lysate version of the APEX2/AUR assay, stimulation of HEK293 cells with agonist to drive trafficking of the DOR to the lysosome caused a loss of signal in the intact version of the APEX2/AUR assay (Fig. 1E). To validate that this loss of signal was due to trafficking of the DOR, we used siRNAs to knockdown β-arrestin-2, a protein critical for DOR endocytosis and access to the endosomal-lysosomal pathway (Extended Data Fig. 3A–B).[22] In cells treated with control siRNA, agonist stimulation before the APEX2/AUR reaction resulted in an ~80% reduction in fluorescence of the cell population while, comparatively, knockdown of β-arrestin-2 strongly inhibited agonist-induced loss of fluorescence (Fig. 1E–F).

We then sought to determine if APEX2 is sensitive to the proteolytic environment of lysosomes, its low pH (4.5–5.0), or both. To test our hypothesis that APEX2 is susceptible to lysosomal proteolysis, we stimulated cells stably expressing DOR-APEX2 with the agonist DADLE for different times before harvesting cells for western blot. Probing with an anti-APEX antibody, we found that the DOR-APEX2 transgene (71 kDa) underwent two observable proteolytic events: an initial cleavage of 10 kDa leaving an ~60 kDa product followed by proteolysis of this intermediate and no further observable anti-APEX immunoreactive species (Fig. 1G, Extended Data Fig. 3C). We then compared the rate of agonist-induced DOR-APEX2 proteolysis to that of agonist-induced signal loss in the DOR-APEX2/AUR assay. We found that the rate of loss of APEX2/AUR signal in the lysate assay fell between that of the initial proteolytic event and total proteolysis, demonstrating the APEX2/AUR lysate assay tracks with the kinetics of APEX2 proteolysis (Fig. 1H). We also found the intact assay lost signal slightly faster than the lysate assay but the difference was not significant (Extended Data Fig. 3D). Finally, we examined if APEX2 activity is sensitive to pH by performing the lysate assay over a pH range of 4.5–7.5. We measured a pKa for

APEX2 activity of ~5.9 (Fig. 1I). Thus, APEX2 activity is rapidly quenched upon delivery to the lysosome, likely by a combination of low pH and proteolytic activity. Together, these data demonstrate that the GPCR-APEX2/AUR assay can be utilized in a high-throughput lysate format, or intact format for single-cell techniques, to measure agonist-induced GPCR downregulation resulting from trafficking to the lysosome.

Genome-wide CRISPR interference screen

We next sought to combine our GPCR-APEX2/AUR assay with a genome-wide CRISPR interference (CRISPRi) screen to identify new genes controlling DOR expression and downregulation. We utilized DOR-APEX2 driven by the human UBC promoter, which had the advantages of lower expression than CMV and the ability to function as an internal control as our CRISPRi libraries included sgRNAs targeting the UBC promoter (Extended Data Fig. 4A). We stimulated cells with agonist, performed the APEX2/AUR reaction, and then sorted for the highest (H) and lowest (L) fluorescent quartiles. We detected sgRNAs for every gene and the majority (96.3%) had 5 of 5 detected sgRNAs, suggesting no major bottlenecks in the workflow (Supplementary Table 1). Using the relative frequency data of the sgRNAs between the two populations, we calculated a knockdown phenotype score (called fold-enrichment: $\log_2$ (H/L) populations) and significance p-value score for each gene (Supplementary Table 1). We then estimated a false discovery rate (FDR) and defined genes with an FDR less than 0.05 as a “hit” using the large number of non-targeting controls (NTCs) contained in the library.[23] There were 492 hits: 183 hits with fold-enrichment less than zero (signifying genes which enhanced DOR expression or inhibited trafficking to the lysosome) and 309 hits with a fold-enrichment greater than zero (signifying genes which inhibited DOR expression or promoted trafficking to the lysosome) (Fig. 2A, Supplementary Table 2).

We examined the gene hits known to function in membrane trafficking. Many of these hits were linked to endocytic or endosomal-lysosomal pathways including endosomal-lysosomal Rabs, components of the endosome-lysosome tethering complexes CORVET and HOPS, and subunits of the vacuolar ATPase (Fig. 2B upper panel, Fig. 2C). We also identified components of the secretory pathway including subunits of the multipass translocon and coatomer complexes (Fig. 2B upper panel and Fig. 2C).[24] Lastly, we used gene ontology (GO) analysis to perform a broad survey of the hits from the screen and found categories related to trafficking as well as many which function in gene expression (Extended Data Fig. 4B).

We next asked how many of our hits—which we identified in a model human cell line —were also expressed in neuronal cells known for endogenous DOR expression, human nociceptor sensory neurons.[12] We analyzed a published RNAseq dataset from 12 different types of human nociceptors.[25] We found 93% of the hits from our CRISPRi screen were found in human nociceptors, and vast majority of these RNAs (>97%) were expressed above the 25th percentile of all measured RNAs (Extended Data Fig. 4C–D). Thus, the majority of our hits are genes that are conserved and expressed in multiple cell types.

In analyzing our genome-wide screen, we noticed that several genes known to control DOR endocytic and endosomal-lysosomal trafficking—including *ARRB2* (which encodes

β-arrestin-2), *GRK2*, *GASP1*—were not identified as hits.[6,9,17,26] While this is likely a natural consequence of genetic screening with computationally designed libraries at the genome-wide scale, we selected a single sgRNA from our libraries targeting *ARRB2* for follow-up. Using the APEX2/AUR lysate assay, we found a small but significant effect when this guide was transduced into the UBC:DOR-APEX2 cell line compared to a NTC sgRNA (Extended Data Fig. 4E). This result is consistent with the genome-wide screen data in which sgRNAs targeting *ARRB2* showed a moderate phenotypic effect that did not quite pass the 0.05 FDR threshold (Supplementary Table 1). This observation demonstrates that the absence of a gene from our hit list does not exclude it as a regulator of DOR expression or trafficking. Together, our genome-wide screen represents a genetic view of the DOR life cycle from "cradle to grave" and captured genes necessary for DOR expression, secretory trafficking, and downregulation resulting from agonist-induced trafficking to the lysosome.

We then picked five novel hits not previously known to function with the DOR but linked to endosomal-lysosomal function to test for a role in DOR trafficking to the lysosome: *DNAJC13*, *WDR91*, *SNX24*, *CPNE1*, and *GAPVD1* (Fig. 2B, lower panel).[27–31] Two sgRNAs per gene were independently transduced into cells stably expressing DOR-APEX2 and dCas9-KRAB. Using the APEX2/AUR lysate assay, we observed that sgRNAs targeting *DNAJC13*, *WDR91*, and *SNX24* all inhibited DOR trafficking to the lysosome (Fig. 2D). We also observed significant effects on DOR trafficking with one of the two sgRNAs targeting *CPNE1* (Fig. 2D). Neither of the sgRNAs targeting *GAPVD1* had significant effects, and this is consistent with *GAPVD1* having the weakest effect in the genome-wide screen of the five genes selected for follow-up. Together, these data support the findings of the genome-wide screen and validate three genes newly implicated in agonist-dependent DOR trafficking to the lysosome.

DNAJC13 regulates trafficking of the DOR to the lysosome

One of the strongest hits from our screen and follow up studies was *DNAJC13*, the human homolog of *C. elegans* receptor mediated endocytosis 8 (RME-8). DNAJC13 localizes to early endosomes, and it has been shown to be required for the recycling of several cargo molecules including CI-MPR, Wntless, and Notch receptor.[32–35] Mechanistically, DNAJC13 has been shown to regulate turnover of the endosomal clathrin and SNX1 via its J domain and HSC70, and loss of DNAJC13 has been shown to cause mixing of the degradative and recycling endosomal sub-domains in *C. elegans*.[33–38] However, the literature is conflicted on whether DNAJC13 promotes or inhibits trafficking of membrane proteins to the lysosome (using EGFR as a model cargo), and the role of DNAJC13 in regulating endosomal trafficking of GPCRs has been largely unexplored.[30,39] Consequently, we sought to further understand the role DNAJC13 plays in DOR downregulation.

We first examined how knockdown of DNAJC13 affects DOR trafficking to the lysosome. Consistent with CRISPRi results, we observed that knockdown of DNAJC13 with a siRNA pool or individual siRNAs inhibited agonist-induced loss of the DOR as measured by both the intact and lysate version of the APEX/AUR assay (Fig. 3A–C, Extended Data Fig. 5A–D). To more precisely characterize the effects of DNAJC13 depletion on DOR trafficking to the lysosome, we performed an extended agonist time course. We found that transfecting

cells with the pooled siRNA targeting DNAJC13 impeded DOR trafficking to the lysosome with a 1.6-fold increase in the $t_{1/2}$ (Fig. 3D–E, Extended Data Fig. 5E). These data suggest that knockdown of DNAJC13 results in a kinetic delay in DOR trafficking to the lysosome without causing a total loss of endosomal-lysosomal function. Importantly, we observed that knockdown of DNAJC13 caused no change in total DOR expression, DOR surface expression, or agonist-induced DOR internalization or recycling, suggesting the defect in DOR trafficking was at the endosomal-lysosomal stage (Fig. 3F–G, Extended Data Fig. 5F–G). Lastly, we asked whether this kinetic delay in DOR trafficking to the lysosome perturbed the ability of the DOR to signal. We examined DOR signaling via Gαi and suppression of cAMP and found that DNAJC13 knockdown did not affect DOR signaling (Extended Data Fig. 5H). Together, our results show that DNAJC13 is specifically involved in the post-endocytic trafficking of the DOR to lysosome.

DNAJC13 localizes to DOR-positive endosomes

We next sought to determine if DNAJC13 localizes to DOR-positive endosomes using super-resolution Airyscan microscopy. Using a highly specific antibody to endogenous DNAJC13, we observed that DNAJC13 puncta were consistently found directly adjacent to DOR-positive endosomes (Fig. 4A–B, Extended Data Fig. 6A). As DNAJC13 is known to interact with the WASH complex subunit FAM21, we hypothesized this adjacent location of DNAJC13 might be near the recycling subdomain on DOR endosomes.[35,37,40] To test this hypothesis, we examined a marker of the endosomal recycling subdomain and endosomal tubules, the Retromer subunit VPS35.[41,42] We found that DNAJC13 partially colocalized with VPS35 (Extended Data Fig. 6B–C). To quantify the relative adjacency or colocalization of DNAJC13 with DOR or VPS35, we scored images for adjacency of puncta (see Materials and Methods, Extended Data Fig. 6D for example of scoring). We found a higher degree of adjacency of DNAJC13/DOR signal compared to DNAJC13/VPS35 while Pearson's correlation coefficient showed the analogous result with higher colocalization of DNAJC13/VPS35 (Fig. 4C–D). To put these paired observations in context, we performed Airyscan three-color imaging experiments with DNAJC13, DOR, and VPS35 where DOR marks the endosome limiting membrane and VPS35 marks the recycling domain/endosomal tubule. We observed that DNAJC13 tended to enrich to the base of the VPS35-positive recycling tubule on DOR-positive endosomes (Fig. 4E, Extended Data Fig. 6E). As had been previously observed for non-recycling GPCRs, we did not see DOR entering the VPS35-positive recycling tubule.[40] To further illustrate the localization of DNAJC13, we selected a single endosome with a visually apparent tubule to create a surface rendering highlighting the relative accumulation of the three proteins (Fig. 4F). Together, our results demonstrate that endogenous DNAJC13 localizes to DOR-positive endosomes and enriches at sites known for endosomal actin polymerization promoted by the WASH complex.[35,37,40]

Loss of DNAJC13 remodels the endosomal DOR proteome

Our data suggest that DNAJC13 resides on DOR endosomes and that DNAJC13 function is required to promote DOR downregulation; however, how DNAJC13 supports DOR egress from early endosomes to the lysosome is less clear. As DNAJC13 has been demonstrated to regulate turnover of endosomal proteins in the degradative and recycling sub-domains, we reasoned that loss of DNAJC13 could cause substantial remodeling of the endosomal

proteome which in turn could disrupt DOR trafficking.[34–36,38,43] To test this hypothesis, we turned to proximity labeling. We have previously shown that GPCR-APEX2/BP can be used to capture high-resolution “snap-shots” of the local proteome around an agonist-activated GPCR.[9] Specifically, APEX2-mediated proximity labeling covalently tags proteins in a ~20 nm window in a thirty-second labeling reaction performed in living cells, and changes in labeling of this proximal proteome can be determined using tandem-mass tagging (TMT) mass spectrometry (Fig. 5A).[8,9]

We first confirmed—consistent with our imaging experiments—that the local proteome of DOR-APEX2 after 15 minutes of agonist is highly endosomal (Fig. 5B, Supplementary Table 3). We then compared the DOR proximal proteome in cells treated with control siRNA or siRNA targeting DNAJC13. We identified 13 proteins as significantly changed in the local proteome of DOR following depletion of DNAJC13 (Fig.5C, Extended Data Fig. 7A and Supplementary Table 4). Unsurprisingly, the protein that showed the strongest depletion from the local DOR proteome was DNAJC13 itself (Extended Data Fig. 7B, Supplementary Table 4). We were particularly intrigued by changes in two proteins known to be important endosomal trafficking: AGAP1 (an endosome-localized ArfGAP) and FAM21 (a subunit of the endosomal actin-polymerizing WASH complex).

AGAP1 has been shown to localize to endosomes and affect trafficking through the endosomal-lysosomal pathway through control of coat complex AP-3 and Arf GTPases at endosomes.[44–46] We found that knockdown of DNAJC13 resulted in an increase in both AGAP1 and Arf1/Arf3 levels in the endosomal DOR proximal proteome (Fig. 5C red circles, 5D, Extended Data Fig. 7C). These observations suggest that an increase in local AGAP1 levels could contribute to defects in DOR trafficking. To test this hypothesis, we examined the effect of overexpression of AGAP1 on DOR trafficking and found DOR trafficking to the lysosome partially inhibited upon AGAP1 overexpression (Fig. 5E, Extended Data Fig. 7D).

We then turned our attention to FAM21, a subunit of the WASH complex. The WASH complex promotes the formation of endosomal branched actin, and loss of WASH function disrupts endosomal and lysosomal morphology.[47–50] Additionally, recent work has demonstrated FAM21 stimulates actin assembly at the endosome by removing the capping proteins from the ARP1 mini-filament of dynactin.[51] In our proximity labeling experiments, we observed that knockdown of DNAJC13 caused a reduction of FAM21 in the endosomal DOR proximal proteome as well as increased levels of two proteins downstream of FAM21 function: ARP1 and actin (Fig. 5C orange circles, 5F, Extended Data Figure 8A–B). While FAM21 is known to interact with DNAJC13, FAM21 recruitment to endosomes relies on Retromer and SWIP but not DNAJC13.[52–55] Thus, we hypothesized that the changing levels of FAM21, ARP1, and actin upon DNAJC13 depletion were due to a change in FAM21 activity at endosomes.[52–54] To test that hypothesis, we turned to a known dominant-negative mutant of FAM21 (FAM21-DN: also called FAM21-tail, $FAM21_{228–1347}$) which competes for the interaction between Retromer and the endogenous WASH complex and causes WASH to be displaced from endosomes.[53,54] Similar to knockdown of DNAJC13, we found that FAM21-DN expression disrupted DOR trafficking to the lysosome both at 2 hours and across a 6 hour time-course (Fig. 5G, Extended Data Fig. 8C–D). We also investigated the

effects of FAM21 knockdown, but our knockdown only achieved moderate loss of FAM21 protein and a trending but statistically insignificant effect on DOR trafficking as analyzed by the APEX2/AUR assay (Extended Data Fig. 8E–F). These observations suggest that either a near complete disruption of WASH is required to disrupt DOR trafficking or, as DNAJC13 is a known interactor of the FAM21 tail, that FAM21-DN also affects DNAJC13 activity (although DNAJC13 recruitment to endosomes does not depend on FAM21).[37] These data demonstrate that DNAJC13 controls a web of interactions at the endosome and that the defects in DOR trafficking following DNAJC13 depletion arise, at least in part, from perturbations to the WASH complex subunit FAM21 and the ArfGAP AGAP1.

DNAJC13 knockdown causes expansion of DOR endosomes

Considering that DNAJC13 knockdown altered the endosomal proteome, we anticipated that loss of DNAJC13 could affect overall endosomal homeostasis. Using super resolution imaging, we found in control cells that the DOR localized to vesicles enriched for the early endosome marker EEA1 following 15 minutes of agonist treatment (Fig. 6A). Strikingly, in cells depleted of DNAJC13 with a siRNA pool or individual siRNAs, DOR-positive early endosomes were much larger than in control cells (Fig. 6A, Extended Data Fig. 9A–C). We quantified the expansion/vacuolation of these DOR/EEA1 positive endosomes and found an ~30% increase in the average diameter (control: 0.78±0.33 μm; siDNAJC13:1.05±0.55 μm) (Fig. 6B). We then created surface renderings of the EEA1-positive DOR endosomes and used these rendering to estimate the volume of endosomes in an unbiased manner (Fig. 6C). We analyzed the volume of over 7,500 structures which were positive for both the DOR and EEA1. We found that the average observed volume of DOR endosomes increased from 0.35 μm^3 to 0.50 μm^3 upon depletion of DNAJC13 (Fig. 6D). Intriguingly, the majority of this effect came not from a change in the median endosome size (which showed a slight decrease upon DNAJC13 knockdown from 0.15 μm^3 to 0.11 μm^3) but from an increase in the largest endosomes in the population. We observed an ~2-fold increase in mean volume in the largest 10% of endosomes in each population (siRNA-control: 1.65 μm^3; siRNA-DNAJC13: 3.04 μm^3) (**Extended Data Fig. D**). Together, these data suggest that, upon DNAJC13 depletion, endosomes become more heterogenous, endosomal homeostasis is disrupted, and a subset of DOR-positive endosomes undergo a dramatic expansion of size.

Given our observations that depletion of DNAJC13 disrupts both the endosomal proteome and endosomal homeostasis, we reasoned that DNAJC13 could be required for the trafficking of many GPCRs. To test this hypothesis, we first examined M2 muscarinic receptor (M2R), a GPCR known to undergo agonist-induced trafficking to lysosome. As with DOR, we found that knockdown of DNAJC13 slowed M2R trafficking to the lysosome (Fig. 6E). We then examined two GPCRs known to recycle from endosomes: the β2-adrenergic receptor (β2AR) and the mu opioid receptor (MOR). We found that knockdown of DNAJC13 caused a reduction in recycling of the β2AR and the MOR (Fig. 6F–G). Together, these results demonstrate that DNAJC13 plays a critical role in GPCR sorting at the endosome, modulating agonist-induced GPCR trafficking to the lysosome as well as GPCR recycling back to the cell surface. We suggest a working model for GPCR endosomal trafficking in which DNAJC13 regulates the activity or local levels of multiple endosomal proteins including FAM21 and AGAP1 and that loss of this function causes

disruptions to the endosomal proteome, endosomal homeostasis, and sorting of GPCRs into recycling or degradative pathways (Fig. 6H).

Discussion

A fundamental cell biological question is how agonist-activated GPCRs are regulated via trafficking through the endosomal-lysosomal pathway. To address this challenge, we have developed a new biosensor, GPCR-APEX2/AUR, to monitor agonist-induced trafficking of GPCRs to the lysosome. This new assay has a large linear range, is highly tunable, and has a ~200-fold better signal-to-noise compared to GFP. We show that APEX2 is sensitive to lysosomal pH and is rapidly proteolyzed in lysosomes, which is in contrast to fluorescent proteins that are often partially or fully resistant to lysosomal proteolysis.[56,57] While we have focused our sensor on monitoring GPCR trafficking to the lysosome, we anticipate that it might be applicable to other biological processes. For example, biosensors for autophagy have utilized the pH-sensitivity of GFP (pKa~6) to develops sensors that are quenched upon formation of the autolysosome, and we anticipate that the APEX2/AUR assay could be utilized in a similar manner leveraging the protease and pH sensitivity of APEX2.[58] Together with our GPCR-APEX2/BP approach for proximity labeling, we demonstrate that the GPCR-APEX2 platform is an effective tool for interrogating both genetic and biochemical aspects of GPCR trafficking by simply switching chemical substrates.

We provide, for the first time, a genome-wide map of the genes required for expression and trafficking of a mammalian GPCR, the DOR. The DOR, a GPCR involved in pain and anxiety, is a prototypical example of a GPCR which undergoes rapid trafficking to the lysosome and downregulation following activation with agonist. Our genome-wide screen identified multiple known players through the endosomal-lysosomal pathway including proteins involved in endocytosis (GRK6, CLTC, DNM2), endosomal sorting (RAB5C, RABEP1, CHMP6), endosome-lysosome fusion (HOPS complex, Rab7), and acidification of the lysosomes (V-ATPase subunits). We validated three new proteins which function with the DOR in its trafficking through the endosomal-lysosomal pathway: WDR91, SNX24, and DNAJC13. Based on known functions, several of these hits—including DNAJC13—are not likely to physically contact DOR but instead are pathway-essential proteins critical for DOR to reach the lysosome. As studies utilized model human cells, a role for our hits in DOR trafficking in native neurons is as of now unexplored, although we show that the majority of the genes we identified are expressed in human nociceptors known for DOR function.[12,25] Lastly, a long-term question in DOR physiology is if agonist-induced trafficking of the DOR to the lysosome on the cellular level drives development of pharmacological opioid tolerance in animals.[59–62] We suggest that the genetic mapping, such as we do here, will be an important step in testing that hypothesis by identifying specific genetic manipulation of DOR trafficking at the endosome.

We focused on understanding the role DNAJC13 plays in DOR trafficking to the lysosome because DNAJC13 function in membrane protein downregulation had been debated and its role in GPCR trafficking unexplored.[30,39] We show that DNAJC13 functions after DOR endocytosis and localizes to DOR-positive endosomes where it promotes DOR downregulation. Importantly, we show that DNAJC13 function is not specific to the

DOR, and DNAJC13 also controls endosomal sorting other degrading GPCRs (M2R) and recycling GPCRs (β2AR and MOR). Thus, DNAJC13 is a dual-function protein promoting GPCR sorting into both the degradative and recycling pathways out of the endosome. How does DNAJC13 promote sorting of GPCRs and other membrane proteins into two opposing pathways out of the endosome? While the mechanism has not been fully resolved, multiple studies have provided key details. On a morphological level, loss of DNAJC13 has been shown to cause the formation of elongated endosomal recycling tubules in human cells and mixing of the recycling and degradative endosomal sub-domains in *C. elegans*.[37,38] We observed that loss of DNAJC13 caused expansion of a subset of DOR-positive endosomes, suggesting a defect in membrane egress through these endosomes, and our finding is consistent with observations in *Drosophila melanogaster* in which loss of DNAJC13 function causes the formation of enlarged Rab4-, Rab11- or Rab7-positive endosomes.[63] On a mechanistic level, DNAJC13—via its J domain and HSC70—has been shown to affect the turnover of clathrin in the endosomal degradative subdomain and SNX1 in the recycling subdomain.[33–38] Our high-resolution proximity labeling of DOR-positive endosomes adds to this model by demonstrating that DNAJC13 regulates multiple endosomal proteins including an Arf and ArfGAP (Arf1/3 and AGAP1), a WASH complex subunit (FAM21), and proteins downstream of WASH complex activity (ARP1, actin). Considering that DNAJC13 is not required to recruit FAM21 to endosomes, the increase in APR1 and actin levels suggest that DNAJC13 may act as a negative regulator of FAM21/WASH function on endosomes.[52–55] Consistent with the DNAJC13-WASH axis being important with DOR trafficking to the lysosome, we observed DNAJC13 localizing to the base of endosomal tubules (where branched actin is known to polymerize) and we found several other genes which operate with WASH as hits in our CRISPRi screen (ARP2, CAPZA, CAPZB, Supplementary Table 4).[40,51] While we did not observe changes in SNX1 or clathrin levels in the DOR proximal proteome, DNAJC13 has been linked to turnover of these proteins rather than overall abundance changes.[33–38] While further studies will be required to show if AGAP1, FAM21, and other proteins identified in our proteomics are the target of the J domain of DNAJC13, our results demonstrate that DNAJC13 controls a larger number of endosomal proteins than previously appreciated. Together, our genetic screen and mechanistic studies demonstrate that the DOR lifecycle is regulated by the concerted action of many proteins and that DNAJC13 operates at early endosomes to coordinate the activity of endosomal recycling and degradative pathways to allow for effective DOR downregulation in response to agonist activation.

Materials and Methods

Chemicals

DADLE ([D-Ala2, D-Leu5]-Enkephalin acetate salt) was purchased from Sigma Aldrich (Cat #E7131), resuspended at 10 mM in ddH_2O, and stored as frozen aliquots at −20 °C. Naloxone hydrochloride was purchased from Tocris (Cat #0599), dissolved in ddH_2O at 10 mM, aliquoted and stored at −20 °C. Chloroquine diphosphate salt was purchased from Sigma Aldrich (Cat #C6628) and dissolved in ddH_2O at 100 mM. This chloroquine working stock was filtered and kept at 4 °C for 1 week. Amplex UltraRed was purchased from ThermoFisher Scientific (Cat #A36006), dissolved in anhydrous DMSO with a

concentration of 10 mM, aliquoted, protected from light, and stored at −20 °C. Hydrogen peroxide (30% w/w) was purchased from Sigma Aldrich (Cat #H1009) and diluted into ddH_2O immediately before use. Bovine serum albumin, fatty acid free, was purchased from Sigma Aldrich (Cat #A7030), dissolved in PBS, and filtered before use. D-luciferin was purchased from GoldBio (Cat #LUCNA-1g), dissolved in 10 mM HEPES pH 7.4 at 100 mM, sterile filtered, aliquoted and stored at −80 °C. Isoproterenol was purchased from Sigma-Aldrich (Cat # I6504), dissolved in 100 mM L-ascorbic acid at 10 mM, aliquoted and stored at −20 °C. Biotin-phenol was purchased from Sigma Aldrich (Cat #SML2135), dissolved in DMSO at 500 mM, and aliquots were stored at −20 °C.

Antibodies

M1 anti-FLAG was purchased from Sigma Aldrich (Cat #F3040, 1:1000). M1 conjugated to Alexa Fluor 647 (M1–647) with an amine-reactive labeling kit from ThermoFisher Scientific (Cat #A20173). Anti-APEX (anti-L-ascorbate peroxidase 2) was purchased from Abcam (Cat #ab222414, 1:1000 for WB, 1:750 for IF). Anti-GAPDH was purchased from EMD Millipore (Cat #MAB374, 1:1000). Anti-DNAJC13 was purchased from Fisher Scientific (Cat #70–277-3, 1:1000 for WB, 1:750–1:1000 for IF). Anti-VPS35 (Cat #NB100–1397, 1:500 for IF), anti-FAM21 (Cat # NBP2–57472, 1:1000 for WB), anti-AGAP1 (Cat # NBP2–15305, 1:1000 for WB) were purchased from Novus Biologicals. Anti-EEA1 (Cat#48453S, 1:500 IF) and anti-β-arrestin-2 (Cat #3857, 1:1000 WB) were purchased from Cell Signaling Technologies. The following secondary antibodies were purchased from Invitrogen: Goat anti-Rabbit 488 (Cat#A32731, 1:1000), Goat anti-Rabbit 555 (Cat#A21428, 1:1000), Goat anti-Mouse 555 (Cat#A32727, 1:1000), Goat anti-Mouse 647 (Cat#A21235, 1:1000), Donkey anti-Goat 647 (Cat#A32849, 1:1000). The following secondary antibodies were purchased from Bio-Rad: StarBright Blue 700 Goat Anti-Rabbit (Cat # 12004161, 1:3000), StarBright Blue 700 Goat Anti-Mouse (Cat # 12004158, 1:3000), StarBright Blue 520 Goat Anti-Rabbit (Cat # 12005869, 1:3000), and StarBright Blue 520 Goat Anti-Mouse (Cat # 12005866, 1:3000). LI-COR: IRDye® 680RD Donkey anti-Rabbit IgG (Cat #926–68073, 1:3000) and IRDye® 800CW Donkey anti-Mouse (Cat #926–32212, 1:3000) were purchased from LI-COR.

siRNA

siRNA targeting β-arrestin-2 (ARRB2–12, Cat #SI03099103) and a non-targeting control (AllStars, Cat # 1027415) were purchased from Qiagen. A pool of 4 siRNAs targeting human DNAJC13 was purchased from Dharmacon/Horizon Discovery (Cat #L-010651–01) as well as the individual siRNAs making up that pool: #9 (Cat #L-010651–09), #10 (Cat #L-010651–10), #11 (Cat #L-010651–11), and #12 (Cat #L-010651–12). A pool of 4 non-targeting siRNAs was also purchased from Dharmacon/Horizon Discovery (Cat #D-001810–10). Two separate pools of 4 siRNAs targeting FAM21A (Cat #L-0262372–01) or FAM21C (Cat #L-029678–01) were purchased from Dharmacon/Horizon Discovery. siRNAs were resuspended in either RNase-free water or RNase-free water (Cat# B-003000-WB) supplemented with siRNA buffer (Cat # B-0020000-UB) purchased from Dharmacon/Horizon Discovery.

cDNA constructs

CMV:DOR-APEX2 is encoded by the construct pcDNA3.1-SSF(signal sequence FLAG)-DORwt-APEX2.[9] UBC:DOR and UBC:DOR-APEX2 are encoded by the constructs puDNA5-SSF-DORwt or puDNA5-SSF-DORwt-APEX2, respectively. Much of the development of the APEX2/AUR assay used the CMV:DOR-APEX2 construct, while the UBC:DOR-APEX2 construct was used for the biological studies and additional controls. No differences were found between the constructs beyond the lower expression of UBC relative to CMV. puDNA5 was created by using the MluI and ApaI restriction sites to remove the CMV promoter from pcDNA5/FRT and replace it with the human ubiquitin C promoter (UBC). Murine DOR (*OPRD1)* was PCR amplified from pcDNA3.1-SSF-DORwt-APEX2. DOR was cloned into puDNA5 and in-frame with a gBlock encoding a linker (GGGGSGGGG) and APEX2 using In-Fusion to create the final construct, puDNA5-SSF-DORwt-APEX2. UBC:DOR-APEX2-eGFP was cloned into puDNA5 using NheI and BamHI restriction sites with DOR-APEX2 PCR amplified from UBC:DOR-APEX2 and linker-(SAGSAGSAG)-eGFP PCR amplified from PM-APEX2.[9] CMV:2AR is encoded by the construct pcDNA3-SSF-β2AR and was a gift from Mark von Zastrow. UBC:MOR and UBC:MOR-APEX2 are encoded by the constructs puDNA5-SSF-MOR or puDNA5-SSF-MOR-APEX2, respectively, and were cloned into puDNA5 using NheI and BamHI restriction sites. Murine MOR (*OPRM1)* was PCR amplified from previously published constructs, and linker APEX2 (GGGGSGGGG) was amplified from the APEX2 constructs described above.[11] UBC:M2R-APEX2 was cloned into puDNA5 using the NheI and XhoI restriction sites and a gBlock encoding M2R (*CHRM2)* and linker-APEX2 PCR amplified from SSF-DORwt-APEX2. CYTO-APEX2 (GFP-APEX2-NES) was cloned into puDNA5 using NheI and NotI restriction sites of puDNA5.[9] cAMP sensor is encoded by GloSensor20F-IRES Rluc.[64] dCAS9 is encoded by the construct pHR-SFFV-dCas9-BFP-KRAB.[65] sgRNAs were cloned into pU6-sgRNA-EF1alpha-puro-T2A-BFP using the BstXI and BlpI restriction sites (see Supplementary Table 5 for a full list of sgRNA sequences and oligos).[3] FAM21-DN was PCR amplified from GFP-BioID-FAM21 (*WASHC2A,* Addgene #121046) with overlaps to clone in frame of mApple in pmApple-C1 between the EcoRI and KpnI sites using NEBuilder. AGAP1 was PCR amplified from a cDNA from Xenopus laevis (DNASU XlCD00708343) with overlaps to clone into pCDNA5 between the NheI and KpnI sites using NEBuilder (a silent mutation was introduced into the oligos to alleviate high Tm secondary structure).

Cell Culture and Stable Cell Line Generation

HEK293 cells (CRL-1583, ATCC), and FLP-In-293 (HEK293-FLP) cells purchased from Thermo Fisher Scientific (Cat # R75007), were cultured in DMEM (Cat #11965–092, Thermo Fisher Scientific) supplemented with 10% FBS and grown at 37 °C with 5% CO_2. No additional authentication was performed for these cell lines. HEK293 cells stably expressing CMV:DOR-APEX2 or CMV:β2AR were maintained in 1:1000 G418/Geneticin (Thermo Fisher Scientific, Cat # 10131035).[9] HEK293 Flp cells stably expressing UBC:DOR-APEX2, UBC:DOR, , UBC:DOR-APEX2-GFP, UBC:MOR, UBC-MOR-APEX2, UBC:M2R-APEX2, or CYTO-APEX2 were created by transient transfection of puDNA5 vector and pOG44 using Lipofectamine 2000 (ThermoFisher Scientific, Cat # 11668019). To ensure sufficient genetic diversity, a ~40% confluent T75 was transfected

to ensure >10 ‘plaques’ grew upon addition and selection with 100 μg/mL hygromycin (ThermoFisher Scientific, Cat #10687010). Cells were maintained in 50 μg/mL hygromycin. To generate HEK293 cell lines stably expressing dCas9, Lenti-X HEK293 cells (Takara Bio, Cat #632180) were transfected with pHR-SFFV-dCas9-BFP-KRAB, pVSVG, and psPAX2 using Lipofectamine 2000. Supernatant was harvested after either 48 or 72 h, filtered through a 0.45 μm PES filter, and incubated overnight with HEK293 FLP cells stably expressing UBC:DOR-APEX2. Cells expressing both DOR and dCas9 were isolated using fluorescence activated cell sorting (FACS) on a BD FACS Aria II (BD Biosciences), serially diluted, and expanded as individual clones. Clones were validated for expression of DOR, dCas9, and activity of dCas9 using sgRNAs targeting the TSS of *ARRB2*.

siRNA transfections

Knockdown of β-arrestin-2 in HEK293 cells was performed using “reverse” transfection in which 20 pmol siRNA (Qiagen) and either RNAimax (ThermoFisher Scientific, Cat #13778075) or Dharmafect1 (Dharmacon, Cat #T-2001–03) were incubated for 20 minutes in OptiMem (ThermoFisher Scientific, Cat # 31985070) and then added to a cell suspension for seeding. Media was exchanged 24 h after transfection and experiments performed 72 h after transfection. Knockdown of DNAJC13 HEK cells was performed using “reverse” transfection in which 19.8–39.6 pmol siRNA (Dharmacon) and 3.33–6.66 μL Dharmafect1 were incubated for 20 minutes in OptiMem and then added to a ~20% confluent cell suspension in one well of a 6-well plate. Cells were lifted and replated 24 h after transfection, and experiments were performed 72 h after transfection. For FAM21 knockdown, siRNA pools targeting FAM21A and FAM21C were mixed in an equimolar ration (9.9 pmol per pool).

Plasmid transfections

HEK293-FLP cells stably expressing UBC:DOR-APEX2 were “reverse” transfected. 0.8 μg-1.2 μg of DNA (pcDNA5, pcDNA5-AGAP1, pmApple-C1-FAM21-CT) and 2 μL Lipofectamine 2000 were incubated in OptiMem for 20 minutes and then added to an ~20% confluent cell suspension in a 24 well plate

Western Blot

Cells were lifted, spun down, then lysed in RIPA (50 mM Tris, 150 mM NaCl, 1% TritonX-100, 0.5% sodium deoxycholate, 0.1% SDS, pH 7.4) supplemented with a protease inhibitor cocktail—which was acquired from ThermoFisher Scientific, either Halt™ Protease Inhibitor Cocktail (Cat #78430) or Pierce Protease Inhibitor Mini Tablets (Cat #A32953), incubated on ice for 10 minutes, sonicated, and centrifuged at 10,000 × g for 10 minutes. Supernatant was mixed with sample loading buffer supplemented with either Invitrogen Bolt reducing agent or 1% v/v 2-mercaptoethanol (Bio-Rad, Cat #1610710). All non-GPCR samples were heated at 90 °C for 5 minutes. Proteins were separated on Bio-Rad 4–20% Mini-PROTEAN TGX Stain-Free™ Protein Gels (Cat #4568096 or Cat #4568095) in SDS-PAGE Running Buffer (0.2501 M Tris, 1.924 M Glycine, 0.0347 M SDS) or NuPAGE 4–12% Bis-Tris Gel (ThermoFisher Scientific, Cat # NP0321) in NuPAGE MOPS buffer (ThermoFisher Scientific, Cat # NP0001). Bio-Rad gels were stain-free activated prior to transferring to nitrocellulose. Blots were blocked with Bio-Rad Everyblot Blocking Buffer

(Cat #12010020) or Odyssey Blocking Buffer (LICOR, Cat # 927–50000) for 1 h at room temperature, then probed with primary antibody overnight for 2 h at RT or at 4 °C. Blots were washed with either PBS or TBS supplement with 0.1% v/v Tween (supplemented with calcium for anti-FLAG blots), incubated with Bio-Rad StarBright Blue Secondaries or LI-COR Secondary Antibodies at 1:2000–3000 for 1 h at room temperature, washed, and then imaged on a Bio-Rad Chemidoc Imaging System or LI-COR Odyssey Infrared Imaging System. Contrast and brightness were adjusted across the entire blot in ImageJ/Fiji (NIH). For quantification, indicated band intensity was analyzed using ImageLab (Bio-Rad), ImageJ/Fiji (NIH), or ImageStudioLite (LI-COR) using stain-free or GAPDH loading controls for normalization.

Amplex Assay, Lysate

The lysate assay was performed with slight variations depending on the experiment. Generally, HEK293 cells were either unstimulated or stimulated with agonist (10 μM DADLE, DAMGO, or carbachol) for the indicated duration. Technical duplicates were performed for all conditions except for Figures 1B, 3C, and S4D which were performed in technical triplicate. Cells were lysed in well using ice-cold Lysis Buffer (PBS, 0.1% TritonX-100) which was allowed to proceed for 3 minutes at room temperature. 2x Reaction buffer #1 (PBS, 0.1% TritonX-100, 50–200 μM Amplex UltraRed, 200 μM H_2O_2) was then added to the Lysis Buffer and allowed to proceed for 1–2 minutes. The reaction was stopped by adding 3x Quench Buffer (PBS, 30 mM sodium L-ascorbate). Fluorescence measurements, excitation 555 nm and emission 610 nm, were taken using a Spark multimode microplate reader (Tecan). Percent GPCR-APEX2 remaining was calculated as percent remaining fluorescence after agonist treatment compared to cells not stimulated with agonist: $f_{treatment}/f_{no\ agonist} \times 100$. For Figure 1C, 1D, and 1G: HEK293 cells stably expressing CMV:DOR-APEX2 were either unstimulated or stimulated with 10 μM DADLE for indicated duration. For experiments testing the effect of chloroquine, chloroquine was added 30 min prior to agonist stimulation at 100 μM final concentration. Cells were washed 1x with PBS supplemented with EDTA and detached from the 6 well plate with PBS+EDTA. Cells were pelleted with centrifugation, 500 × g for 5 minutes. 2x reaction buffer #2 (PBS, 0.1% TritonX-100, 100 μM Amplex UltraRed, 5 mM H_2O_2 and protease inhibitor cocktail) was added to cell pellet on ice. The reaction was allowed to proceed for 2 minutes at room temperature, and stopped by directly adding 10 mM final of freshly prepared sodium L-ascorbate. For 1C and 1D fluorescence measurements, excitation 485 nm and emission 590 nm, were taken using a Spectra Max Gemini XPS (Molecular Devices). For 1G fluorescence measurements, excitation 561 nm and emission 610 nm, were taken using a Spectra Max Gemini XPS (Molecular Devices).

Linear Range of Amplex Assay, Lysate

For analysis of Amplex Lysate Assay with varying cell numbers, HEK293-FLP cells stably expressing UBC:DOR-APEX2 were washed with PBS, detached with TrypLE Express (ThermoFisher Scientific, Cat # 12604039), and centrifuged with an equivalent volume of DMEM+10% FBS. Cells were counted in Trypan Blue (ThermoFisher Scientific, Cat #15250061) using a Countess FL (Invitrogen) and concentration was determined as the average counts from two areas on both sides of a hemocytometer. Cells were aliquoted into

separate tubes spanning a range of 39,250–1,256,000 cells per reaction. Cell pellets were lysed for 3 min on ice in Lysis Buffer (PBS+0.1% TritonX-100). 2x reaction buffer #2 (PBS, 0.1% TritonX-100, 50–200 μM Amplex UltraRed, 200 μM H_2O_2) was added and the reaction was allowed to proceed for 1 minute before addition of 3x Quench Buffer (PBS, 30 mM sodium L-ascorbate). Quenched lysate was then moved to a 96 well plate (Costar, black half area, Cat # 3694) and fluorescence was measured, excitation 561 +/− 10 nm and emission 610 +/− 10 nm, using a Spark multimode microplate reader (Tecan) with gain optimized each run to the highest signal sample.

Comparison of GFP and Amplex Lysate Assay

HEK293-FLP cells stably expressing UBC:SSF-DOR-APEX2-GFP and non-expressing control HEK293 Flp cells were seeded and lysed in Lysis Buffer (PBS+0.1% TritonX-100) in a 24-well. After lysis, cells were either transferred to an opaque 96-well for plate reader detection of GFP signal or subjected to Amplex Lysate Assay as described above before also being transferred to an opaque 96-well for AUR signal detection. Samples were performed in technical duplicate and fluorescence was measured for GFP (excitation 488 +/− 10 nm and emission 525 +/− 10 nm) or AUR (excitation 561 +/− 10 nm and emission 610 +/− 10 nm) using a Spark multimode microplate reader (Tecan) with gain optimized each run to the highest signal sample.

Naloxone Dose Response Curve in Amplex Lysate Assay

HEK293 Flp cells stably expressing UBC:DOR-APEX2 were plated in 24 well plates at 20% confluence. 48 hours later, cells were treated with naloxone for a final in-well concentration of 100 μM, 30 μM, 10 μM, 3 μM, 1 μM, 300 nM, 100 nM, or 30 nM. Cells were then treated with 30nM DADLE and incubated at 37 degrees C 5% CO2 for six hours. Receptor degradation was measured using the AMPLEX lysate assay as described above. Experiments were performed in technical triplicate and results were normalized to the maximum fluorescence value.

Amplex Assay, Intact Cells

Cells were either unstimulated or treated with agonist before lifting with TrypLE or TrypLE Express and pelleted with DMEM +10%FBS by centrifugation. Cells were resuspended in ice-cold PBS supplemented with 200 μM Amplex UltraRed, incubated at room temperature for 5 minutes followed by 10 minutes on ice. To avoid the potential of any extracellular reaction products interfering with our measurements, the reactions prepared for FACS were performed in the presence of bovine serum albumin (BSA) which has been shown to be highly effective at capturing extracellular resorufin and resorufin-like molecules.[19] 2x Reaction buffer #3 (PBS, 4% w/v BSA, 100 μM H_2O_2) was prepared immediately before use and added directly to cells. Reaction was allowed to proceed for 30 seconds and quenched with the addition of sodium azide, 1 mM final. Cells were pelleted with centrifugation at 500 × g for 1 minute, washed with PBS supplemented with 2% BSA, and then resuspended in PBS supplemented with 1% BSA. Cells were analyzed on a BD FACS Aria II using the following channels: APC (Excitation: 633 nm; Emission:670/30 nm), mCherry (Excitation:561 nm; Emission: 610/20–600 nm LP); PE (Excitation: 488 nm; Em: 575/25–500 nm LP), Pacific Blue (Excitation: 405 nm; Emission: 450/50 nm) or on

Cytoflex S (Beckman Coulter) APC (Excitation: 638 nm; Emission: 660/20 nm). At least 15,000 cells were counted per sample, and singlets were gated for further analysis. For analysis of cell fluorescence was performed in FlowJo (BD Biosciences) using either the median or geometric mean on of the singlet population.

APEX activity as a function of pH

The lysate APEX2/AUR assay was performed as described above except that the HEK293 cells stably expressing DOR-APEX2 were directly lysed with Universal Buffer (20 mM sodium acetate, 20 mM MES, 20 mM HEPES, 100 mM sodium chloride, 0.1% TritonX-100) at the indicated pH for 3 minutes on ice. 2x Reaction Buffer #4 (Universal buffer supplemented with 200 μM Amplex UltraRed, 100 μM H_2O_2) was added directly to the lysis, the reaction occurred for 1 minute, and then quenched with 10 mM final concentration sodium L-ascorbate. To measure the pH dependence of the oxidation product, universal buffer was replaced with PBS for the reaction and the quenched reaction product was added as a 1:10 dilution to the Universal Buffer at the indicated pH. Fluorescence measurements, excitation 561 nm and emission 610 nm, were taken using a Spectra Max Gemini XPS (Molecular Devices). Data were processed by subtracting fluorescence from the buffer alone and normalized to the maximal fluorescence observed for the assay at pH 6.5.

Comparison of Amplex Assay (Lysate vs Intact) and Western blot

HEK293 cells stably expressing CMV:DOR-APEX2 were either unstimulated or stimulated with 10 μM DADLE for 2, 3, 4, or 6h. Cells were washed 1x with PBS+EDTA, detached from the plate with TrypLE Express, and split into three different workflows: lysate APEX2/AUR, intact cell APEX2/AUR, and western blot assays. Fluorescence of both lysate and intact cell assays measured with a Spectra Max Gemini XPS (Molecular Devices), excitation 561 nm and emission 610 nm. Western blot data was acquired using an Odyssey Infrared Imaging System (LI-COR) and quantified with ImageStudioLite (LI-COR).

Effect from DNAJC13 knockdown on Surface expression, Internalization, and Recycling Assays

HEK293-Flp cells stably expressing UBC:DOR, UBC:DOR-APEX2 or UBC:MOR, or HEK293 cells stably expressing CMV:β2AR were transfected with pooled siRNAs targeting DNAJC13 or a non-targeting control as described above. 72 h after transfection, cells were stimulated with agonist (10 μM DADLE for DOR, 10 μM DAMGO for MOR, or 10 μM isoproterenol for β2AR) for noted time for internalization (30 minutes). To measure recycling, a surface expression condition (10 μM naloxone for DOR or MOR or 10 μM alprenolol for β2AR, for 30 minutes) and recycling condition (30 minutes of agonist following by 30 minutes of antagonist) were performed. Cells were washed 1x with PBS (Corning, Cat #21–031-CV), detached from the plate with TrypLE Express, and resuspended in FACS Bufer #2: PBS with calcium and magnesium (Corning, Cat #21–030-CV) supplemented with 1% BSA. Alexa647-conjugated M1-anti-FLAG antibody was incubated with cells for 1 h at 4 °C, washed 1x, and resuspended in FACS Buffer #2. Cells were analyzed in a Cytoflex S (Beckman Coulter) using the following channel: APC (Excitation: 638 nm; Emission: 660/20 nm). At least 10,000 cells were counted per sample,

and singlets were gated for further analysis. The geometric mean of the APC channel was used to quantify surface expression, internalization (1-[agonist/antagonist]), or recycling ([recycling-agonist]/[antagonist-agonist]).

Measurement of DOR-mediated Suppression of cellular cAMP.

HEK293-FLP cells stably expressing UBC:DOR or UBC:DOR-APEX2 were "forward" transfected 24 h before the experiment with 3.5 μg GloSensor20F-IRES-Rluc, 9.6 μL of Lipofectamine 2000, in a 6 well. For experiments examining the effect of DNAJC13 knockdown, cells were "reverse" transfected with siRNA 48 h before transfection with GloSensor20F-IRES-Rluc. On the day of the experiment, cells were resuspended in Imaging Media (30mM HEPES in DMEM w/o phenol red, Gibco A1896702), and incubated with 1.6mM D-Luciferin for 1 hour at 37 °C, 5% CO_2. Cells were then treated with only imaging media with 1.6mM D-Luciferin, imaging media with 1.6mM D-Luciferin and 30 nM isoproterenol (to stimulate cAMP production), or imaging media with 1.6mM D-Luciferin and 30 nM isoproterenol + 10 μM DADLE. For luminescence reads, cells were imaged in a 96-well in a TECAN SPARK 37 °C heated light-proof chamber every 10 s for 10–20 min. Each condition (no treatment, 30 nM isoproterenol, or 30 nM isoproterenol + 10 μM DADLE) was performed in triplicate. For cAMP analysis, the triplicates readings for each timepoint were averaged and the three max values of these averages were obtained for each condition. The three max values were then averaged, and the vehicle average was subtracted from the others. Percent cAMP inhibited was then calculated using these background subtracted values and the formula: (1 − (isoproterenol + DADLE) / isoproterenol) × 100.

Comparison of DOR surface expression between CMV and UBC promoters

HEK293-Flp cells stably expressing UBC:DOR-APEX2 or CMV:DOR-APEX2 were seeded in addition to the parental line and cultured for 24 hours. Cells were approximately 80% confluent when washed 1x with PBS (Corning, Cat #21–031-CV), detached from the plate with TrypLE Express, and resuspended in FACS Buffer #2: PBS with calcium and magnesium (Corning, Cat #21–030-CV) supplemented with 1% BSA. Alexa647-conjugated M1-anti-FLAG antibody was incubated with cells for 1 h at 4 °C, washed 1x, and resuspended in FACS Buffer #2. Cells were analyzed in a Cytoflex S (Beckman Coulter) using the following channel: Excitation: 638 nm; Emission: 660/20 nm. At least 10,000 cells were counted per sample, and singlets were gated for further analysis. The geometric mean of the APC channel was used to quantify surface expression with the parental line establishing a baseline control to subtract background fluorescence ([UBC − Parental] / [CMV − Parental]).

Genome-wide CRISPR interference screen

HEK293-FLP cells stably expressing UBC:DOR-APEX2 and dCas9-BFP-KRAB were transduced, separately, with seven different CRISPRi sgRNA sub-libraries to obtain coverage of the entire human genome (H1-H7).[66] To ensure the majority of transduced cells only contained a single sgRNA (MOI < 1), initial transduction rates were kept below 40% with sufficient cells transduced and grown to ensure >500-fold coverage of the sub-libraries. Two days after transduction, puromycin (Gibco, Cat #A1113803) at a final concentration of 0.75 μg/mL was added for 72 h to select for transduced cells. Cells were allowed to recover

and grow for an additional two days. At 6 days post-transduction, cells were stimulated with 10 μM DADLE for 90 minutes and the intact cell version of the APEX2/AUR assay was performed: cells were washed with PBS+EDTA, detached with TrypLE Express, and centrifuged with an equivalent volume of DMEM+10% FBS. All cells were resuspended in PBS, pooled, divided into 8 fractions, and then processed 4 fractions at a time. 200 μM AUR was added directly to foil-covered cells, incubated for 5 minutes at RT, and then 10 minutes at 4 °C. 2x Reaction buffer #3 (PBS+4% w/v BSA +100 μM H_2O_2) was added to cells, reaction was allowed to proceed for 90 seconds, and then quenched through addition of sodium azide (1 mM final). Cells were centrifuged for 3 minutes at 500 × g at 4 °C, washed 1x with PBS +2% BSA, and resuspended in PBS+1% BSA. All samples were pooled, passed through a 40-μm nylon filter (Corning, Cat #352340), and prepared for FACS on a BD FACS Aria II using the following nested gating scheme: singlets, BFP positive, and the top and bottom quartile of the APC channel. Genomic DNA was harvested from the FACS sorted cells using QIAamp DNA Blood Maxi kit (Qiagen, Cat #51192), sgRNA libraries were prepared using Q5 HotStart High Fidelity (NEB, Cat #M0493L) and barcoding primers (Supplementary Table 5). PCR products were purified using QIAquick PCR purification columns (Qiagen, Cat #28106), loaded onto 20% TBE gels (ThermoFisher Scientific, Cat #EC63155BOX), and an ~270 bp band was excised from the gel. This product was quantified using a Bioanalyzer (Agilent) and sequenced on an Illumina HiSeq-4000 (Illumina) using custom primers (Supplementary Table 5). One biological replicate was performed of this screen.

Bioinformatic Analysis of CRISPRi screen

Next generation sequencing data from the CRISPRi screen was analyzed as follows: each sub-library was analyzed independently as follows: raw sequencing reads were cropped and aligned and filtered by expected libraries. A phenotype score, called fold-enrichment (also called epsilon), was calculated as a log2 ratio using the three strongest sgRNAs per TSS by absolute value. P-values were calculated using a Mann-Whitney test comparing all five sgRNAs targeting a given TSS relative to all non-targeting controls. A composite score (the product of the epsilon and p-value) was used to calculate an FDR with a cutoff of <0.05 and identify high-confidence "hits."[23,67,68]

GO code analysis

The high confidence hits (492 from CRISPRi screen and 101 from proteomic comparison of DOR-APEX2 vs Cyto-APEX2) from the screen were analyzed using the PANTHER overrepresentation analysis for "Slim Cellular Component" with a Fisher's exact test and Bonferroni correction for multiple comparisons. GO categories with statistically significant overrepresentation were ranked by the number of hits found, and any redundant categories (defined as a category with only one unique hit relative to previous categories) were removed. Overly broad categories (e.g., "cellular_component") were also removed.

Analysis of Dorsal Root Ganglia Spatial Transcriptomics Dataset for Expression of CRISPRi Hits

Dorsal root ganglia spatial transcriptomics dataset (21805 genes)—encompassing twelve different cell types—was downloaded (https://sensoryomics.shinyapps.io/RNA-Data/) and

loaded into RStudio.[25] The dataset was searched for the 492 hits from the DOR CRISPRi screen, finding 457 genes. Quartiles were found for each cell type in both datasets, and genes from the hit list were analyzed for RNA expression level measured above the 25th percentile for all RNAs measured in the nociceptor dataset. Additionally, the gene expression level at the 25th percentile was compared across cell lines, between the total dataset and 457 hits using a two tailed t-test.

sgRNA follow up screen

To generate lentivirus for sgRNAs targeting select gene TSS, LentiX HEK293T cells were transfected using Lipofectamine 2000 and the pU6-sgRNA of interest, pPAX2, and pVSVG. Media on 293T cells was changed 24 h after transfection, and viral supernatant was collected and filtered at 48 h after transfection. HEK293-FLP cells stably expressing UBC:DOR-APEX2 and dCas9-BFP-KRAB were transduced, separately, with viruses encoding the different sgRNAs. 2 μg/mL puromycin was added 24 h after transduction to select cells with sgRNAs, and selection was maintained for 3 passages across 7 days. Cells were frozen and thawed to be assayed over ~10 days, after which a new aliquot was thawed. Cells were analyzed using the lysate APEX2/AUR assay as described above.

Fixed Imaging

HEK293-FLP cells stably expressing UBC:DOR-APEX2 were plated onto poly-L-lysine (Sigma Aldrich, Cat # P8920–100ML) coated coverslips in 24-well plates. Cells were fixed for 20 minutes with fixing solution (PBS with 3.7% (v/v) paraformaldehyde (Thermo Scientific, Cat #28906)). PFA was quenched and washed with TBS and the samples were then permeabilized and blocked for one hour with Imaging Buffer (PBS, 3% BSA, and 0.1% TritonX-100). Primary antibodies were added at 1:500–1000 in fresh Imaging Buffer. After labeling for 1 hour at room temperature, the coverslips were washed 3X with PBS and secondary antibodies were added at 1:1000 in Imaging Buffer. After labeling for ~45 minutes, the samples were washed 3X with PBS and cover slips were mounted on glass slides with Prolong Gold Mounting Media (Thermo Scientific, Cat #P36934) and allowed to dry overnight. Samples were imaged on a Zeiss LSM 900 with Airyscan 2. Following Airyscan processing in Zen Blue software (Zeiss), single confocal slice images were processed in FIJI.

Fixed Imaging: Validation of DNAJC13 Antibody

HEK293-FLP cells and HEK293-FLP cells expressing UBC:DOR-APEX2 were siRNA treated according to protocol above. HEK293-FLP cells were treated with non-targeting control siRNA while HEK293-FLP cells expressing UBC:DOR-APEX2 were treated with DNAJC13 siRNA. 24 h following transfection, cells were lifted and replated onto poly-L-lysine coated coverslips in wells of a 24-well plates at equal confluence (~25%). Fixation, staining, imaging of single confocal slices, and processing were performed as described, using Prolong Gold Mounting Media with DAPI (Thermo Scientific, Cat# P36962).

Pearson's Correlation Coefficient

HEK293-FLP cells expressing UBC:DOR-APEX2 were stained for DOR, VPS35, and DNAJC13 as stated above. Pearson's Correlation Coefficient was calculated for DNAJC13/VPS35 and DNAJC13/DOR from z-stack imaging, 3 stacks per slide (technical replicates), with 3 slides per condition (biological replicates). Background subtraction values were obtained by establishing 3 frames not including cellular material and averaging these intensity values. An average Pearson's Coefficient was calculated for each technical replicate by averaging the values from the z-stack slices.

Scoring Adjacency of DOR, DNAJC13, and VPS35

HEK293-FLP cells expressing UBC:DOR-APEX2 were stained for DOR, VPS35, and DNAJC13 as stated above. Single confocal slice super resolution Airyscan images were processed in 3-D in Zen Blue and the images were adjusted for brightness and contrast in FIJI. Slides were fixed in biological triplicate and images were acquired from the two conditions (VPS35/ DNAJC13 and DOR/ DNAJC13). For DOR/ DNAJC13, 10 images were acquired at 63X magnification per biological replicate summating to 30 images processed. As the VPS35/ DNAJC13 condition contained more scorable structures per image, 3–5 images were acquired at 63X magnification per biological replicate summating to 13 images processed. Images were processed, all images were then randomized with a numerical code and given to a blinded reviewer for scoring of "adjacency." Only structures with proximal DNAJC13/DOR or DNAJC13/VPS35 were analyzed. Structures were manually scored as "adjacent" or "overlapping" as follows; Adjacent: 0–49% of DNAJC13 signal colocalizes with signal from VPS35 or DOR. Overlapping: >50% of DNAJC13 signal colocalizes with signal from VPS35 or DOR. Scoring was performed for data obtained from three independent biological replicates with 3–5 images per replicate.

Surface Rendering in Imaris

Super resolution Airyscan images were processed in 3-D in Zen Blue and the file types were converted using Imaris File Converter. The Surfaces tool in Imaris (v10) was utilized to produce 3-dimmensional surfaces for the relevant channels (FLAG (DOR), DNAJC13, and VPS35) or (APEX(DOR) and EEA1). Surface grain size was set to 0.100 μm and surfaces were rendered as partially opaque to view overlap between the channels.

APEX2-Mediated Proximity Labeling and Proteomics

HEK293-Flp cells stably expressing UBC:DOR-APEX2 and UBC:GFP-APEX2 were transfected in biological triplicate with pooled siRNAs targeting DNAJC13 or a non-targeting control (NTC) as described above. 72 hours post transfection, media was replaced with fresh complete media containing 500 μM Biotin-phenol and incubated for 15 minutes. Cells were the stimulated for 15 minutes with 10 μM DADLE. Proximity labeling was initiated by adding 1 mM H2O2 for 30 seconds. Labeling was quenched by aspirating media and replacing with quenching buffer (PBS, 10 mM sodium L-ascorbate, 1 mM Trolox, 10 mM sodium azide) and washed three times before lysing in well with RIPA containing HALT protease inhibitor, sodium L-ascorbate and Trolox. Lysates were sonicated, clarified, and bound overnight at 4 °C to 250 μL streptavidin resin before extensive washing, reduction

with 5 mM TCEP for 30 min at 55 °C, alkylation with 10 mM iodoacetamide for 20 min at RT and on bead trypsinization overnight at 37 °C. Peptides were then purified using a MacroSpin C18 column (The Nest Group,Part # SMMM SS18V). Purified peptides were quantified using the Pierce Quantitative Colorimetric Peptide Assay (Thermo Scientific, Cat # 23275) and 15 μg of peptide from each sample were labeled using a TMTpro 18-plex Label Reagents (Thermo Scientific, Cat # A52047). A small amount of each sample was pooled, dried down, and resuspended and analyzed by a 140-min LC-MS/MS method using the Orbitrap Fusion Tribrid mass spectrometer (Thermo Fisher Scientific) to normalize total reporter ion intensity of each sample. Using normalization factors from this initial run, equal-total intensity volume aliquots of samples were pooled to achieve the desired amount of digest for the 2D-RPRP experiment, dried down, and resuspended. Pooled, dried, and resuspended TMTpro labeled peptides were analyzed by LC-MS on a Dionex Ultimate HPLC operating in 2-D mode couple to an Orbitrap Fusion Tribrid mass spectrometer (Thermo Fisher Scientific) using the SPS MS3 scan mode for TMT quantification. Using the PAW pipeline[69] and COMET search engine (versions 2016.03)[70], spectra were extracted and searched against a UniProt human database with added contaminants (downloaded April, 2020, 20605 protein entries plus 174 common contaminant sequences plus sequence-reversed decoys). Comet was configured with static modifications for TMTpro reagents (+304.2071 Da) on lysines and peptide N termini, static cysteine alkylation (+57.0215 Da), variable oxidation of methionine, parent ion mass tolerance of 1.25 Da, fragment ion mass tolerance of 1.0005 Da, and fully tryptic digest with a maximum of 2 missed cleavages. Identified peptides were filtered using a reversed sequence decoy strategy[71] to control peptide-spectrum-match (PSM) false discovery at a 1% false discovery rate. At least two unique peptides were required for identification of a protein from data. List of inferred proteins and TMT reporter ion intensities were then exported for statistical analyses. Total reporter ion intensities were compared between groups using the Bioconductor package edgeR[72] after trimmed mean of M-values normalization[73] within RStudio. Multiple testing corrections and calculation of false discovery rates were performed by edgeR and hits were selected based on an <10% false discovery rate.

Effect from DNAJC13 Knockdown on Endosome Size Analyzed with Imaris and FIJI

Samples were stained for DOR (anti-APEX) and EEA1 (anti-EEA1) and imaged on a Zeiss LSM 900 with Airyscan 2. For Fig. 6B: a single z plane containing multiple cells was selected as representative, the image was processed in FIJI, and coded for scoring. Images were scored based on the following rules: 1) Only DOR structure needed to be greater than 333 nm were scored so that size measurements were accurate; 2) DOR structure needed to co-localize with EEA1; 3) Longest diameter of structure was measured; 4) If it was unclear if DOR/EEA1 structure was a contiguous compartment, structure was not scored. For Fig. 6D: prior to acquiring the images, slides were uniquely coded to ensure blinded acquisition and analysis for endosomal size. Prior to acquiring the images, slides were uniquely coded to ensure blinded acquisition and analysis for endosomal size. Samples were imaged on a Zeiss LSM 900 with Airyscan 2. Following Airyscan processing in Zen Blue software (Zeiss), images were analyzed in Imaris where surfaces were generated for the APEX-2 channel and EEA1 channel. To identify cargo-positive endosomal structures of interest, the surfaces in the APEX-2 (DOR channel) were filtered by the ratio of their

volume overlapping with EEA1 surfaces. An empirical ratio was derived using 2%, meaning that any DOR surface with 2% of its total volume overlapping with an EEA1 surface was utilized in our data set. Using the filtered population of cargo-positive endosomal structures, we calculated endosomal volumes for every structure in our fields.

Statistical Analysis and Reproducibility.

Statistical analysis for cell biological experiments was performed in Prism (Graphpad) or published software for proteomics (PAW pipeline) and genomics (CRISPR_FACS_v1.6), and all relevant information is provided in the figure legends.[23,67] All data are independent biological experiments or a mean ± s.d. from three independent biological experiments. All experiments were reproduced at least two times except for the genome-wide CRISPRi screen which was performed once across seven independent sub-libraries, and all N (independent biological experiments) are noted in the figure legends. Each biological replicate of the APEX2/AUR-lysate assay is an average of at least two technical replicates processed in parallel. All measures were taken from distinct samples with the following exceptions: 1) Ext. Fig 5D replots Fig. 3C with additional data from siRNAs #11 and #12 added; 2) Fig. 5E and 5G share n=2 pcDNA5 controls which were measured on the same day and shared between datasets; 3) Ext. Fig. 9D is a replot of the top 10% (the 90th percentile) from Fig. 6D. Symbolic representation of p values are as follows: ns=p>0.05, *=p≤0.05, **= p≤0.01, ***= p≤0.001, ****= p≤0.0001

Software and Code

Data were collected with the following software (most recent version listed): microscopy (Zen v3.5), plate-reader (SoftmaxPro cerca 2016–2017 or Tecan Spark Control, v3.0), western blot (LI-COR Acquisition circa 2016–2017 or BioRad Image Lab Touch, v2.4.0.03), flow cytometry (BD FACSDiva v8.0 or Beckman Cyt Expert v2.4). Data were analyzed with the following software (most recent version listed): statistical analysis and graphing (Graphpad Prism, v10), imaging—micrographs (Fiji, ImageJ2 v2.9.0/1.53t), imaging—surface rendering and volume analysis (Imaris, v10), flow cytometry (FlowJo v9 or v10), proteomics (PAW pipeline (https://github.com/pwilmart/PAW_pipeline) and Comet search engine (v2016.03), reporter ion intensities were compared for statistical analysis with edgeR (3.40.0) in RStudio (2022.07.2, Build 576)), and genome-wide screen NGS data (open-source custom software, CRISPR_FACS_v1.6).[23,67]

Extended Data

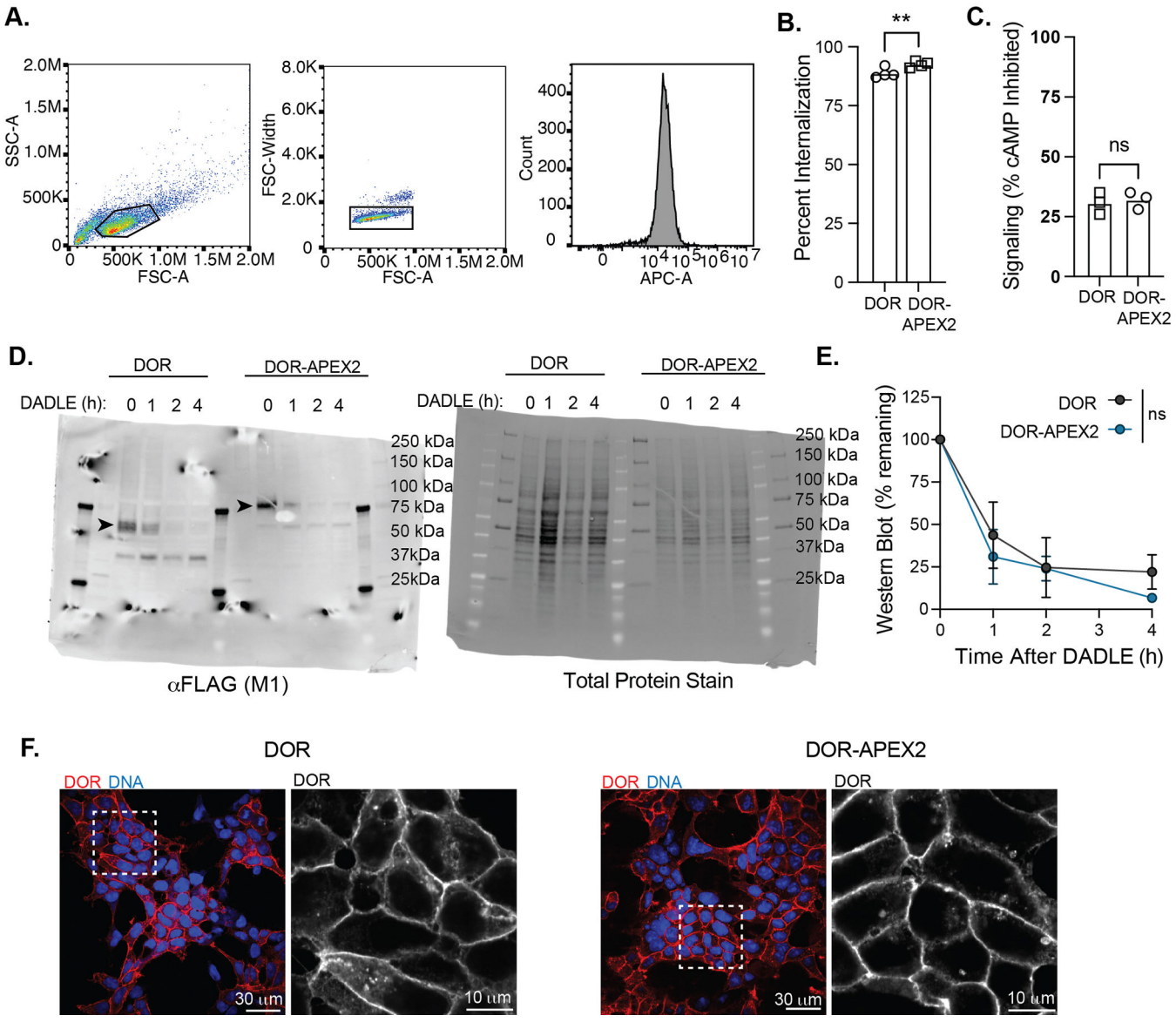

Extended Data Figure 1: DOR is amenable to a C-terminal APEX2 tag.

(a) Example of the flow cytometry gating strategy. Cells were gated by size (cells analyzed: 15510), singlets (cells analyzed: 10114), and then analyzed for fluorescence (cells analyzed: 9744). (b) DOR internalization in HEK293-FLP cells stably expressing UBC:DOR or UBC:DOR-APEX2 analyzed following 30 minutes treatment with the agonist DADLE (10 μM). Agonist induced changes in cell surface DOR between treated and untreated cells was probed with anti-FLAG immunoreactivity and measured with a Beckman Coulter Cytoflex S. N=4 independent experiments, and data were analyzed using a two-tailed paired t-test (p=0.0094). (c) DOR signaling was measured as suppression of cAMP and assayed in HEK293-FLP cells stably expressing UBC:DOR or UBC:DOR-APEX2 and transiently expressing pGLO-20F-IRES-RLUC (pGLO). Cells were simultaneously treated

with the agonist isoproterenol (30 nM) to stimulate the endogenous B2AR and the DOR agonist DADLE (10 μM). cAMP levels were probed via the pGLO sensor and sensor luminescence was measured using a Tecan Spark, N=3 independent experiments, and data were analyzed using a two-tailed paired t-test. (d,e) DOR proteolysis in HEK293-FLP cells stably expressing UBC:DOR or UBC:DOR-APEX2 were analyzed by western blot (M1 anti-FLAG; constructs have N-terminal FLAG tag). (d) Cells were treated with agonist DADLE (10 μM) for the indicated time before lysis and western blot. (e) Loss of the major band (arrow shown in (d)) was quantified N=3 independent experiments shown as mean ± SD and analyzed by a two-way ANOVA across the time-course (alpha=0.05). (f) HEK293-FLP cells stably expressing UBC:DOR or UBC:DOR-APEX2 were fixed, permeabilized, and probed for DOR (M1 anti-FLAG; constructs have N-terminal FLAG tag) and DNA (DAPI). Wide-field (30 μm scale bar; DOR red and DAPI blue) and zoomed (10 μm scale bar; DOR greyscale) images are shown from a confocal slice taken on an Andor BC43 microscope. White box represents area in wide-field selected for zoom, N=2 independent experiments, representative image shown.

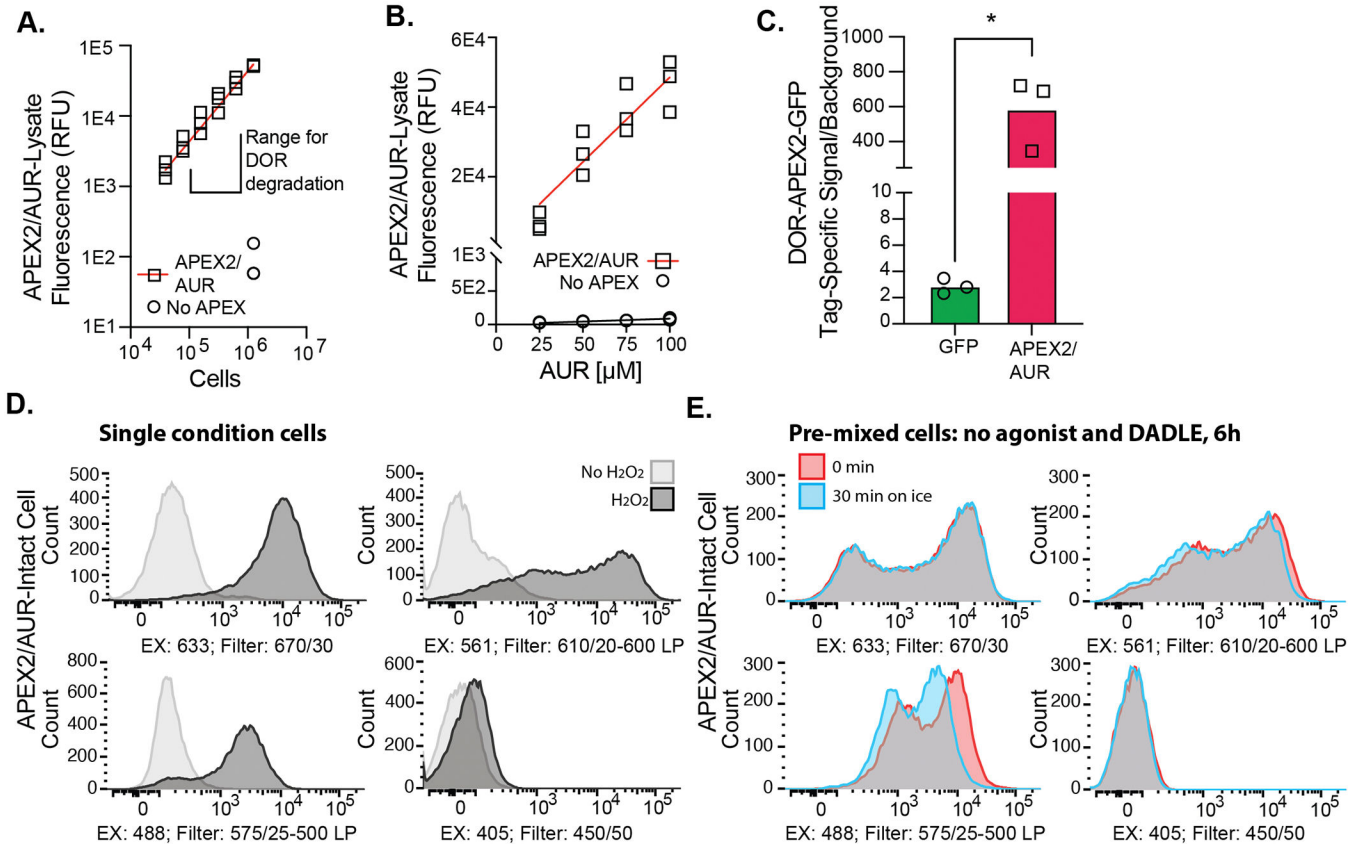

Extended Data Figure 2: APEX2-based fluorescence biosensor for GPCR downregulation.

(a) Linear range of APEX2/AUR lysate reaction was probed with specific numbers of HEK293-FLP cells stably expressing UBC:DOR-APEX2 or non-expressing control. Standard range for examining DOR trafficking to the lysosome for this cell line shown in brackets. N=3 independent experiments, linear regression fit to the data and constrained to the origin. (b) Tunable signal-to-background of the APEX2/AUR lysate assay was

probed by varying the concentration of AUR in HEK293-FLP cells stably expressing UBC:DOR-APEX2-GFP or a non-expressing control. N=3 independent experiments, linear regression fit to the data and constrained to the origin. (c) Comparison of APEX2/AUR and GFP signal-to-background was analyzed in HEK293-FLP cells stably expressing UBC:DOR-APEX2-GFP or a non-expressing control. Assay specific signal was measured in a Tecan Spark plate reader is plotted. N=3 independent experiments, and data were analyzed using a two-tailed paired t-test (p=0.0396). (d) Single cell analysis of APEX2/AUR intact assay (H202, dark grey) or no reaction conditions (no H202, light grey). Cells were analyzed on a BD FACS Aria II, N=2 independent experiments, representative example shown (cells analyzed: 21818 (No H202) or 22062 (H202)).(e) Single cell analysis of stable deposition of reaction product(s) of the APEX2/AUR assay in HEK293 cells stably expressing CMV:DOR-APEX2. Two populations of cells (unstimulated or stimulated by DADLE for 6 hours) were mixed prior to the APEX2/AUR assay, and analyzed on a BD FACS Aria II immediately following the reaction (red) or after 30 minutes on ice (blue). N=2 independent experiments, representative example shown (cells analyzed: 20690 (0 min) or 20794 (30 min)).

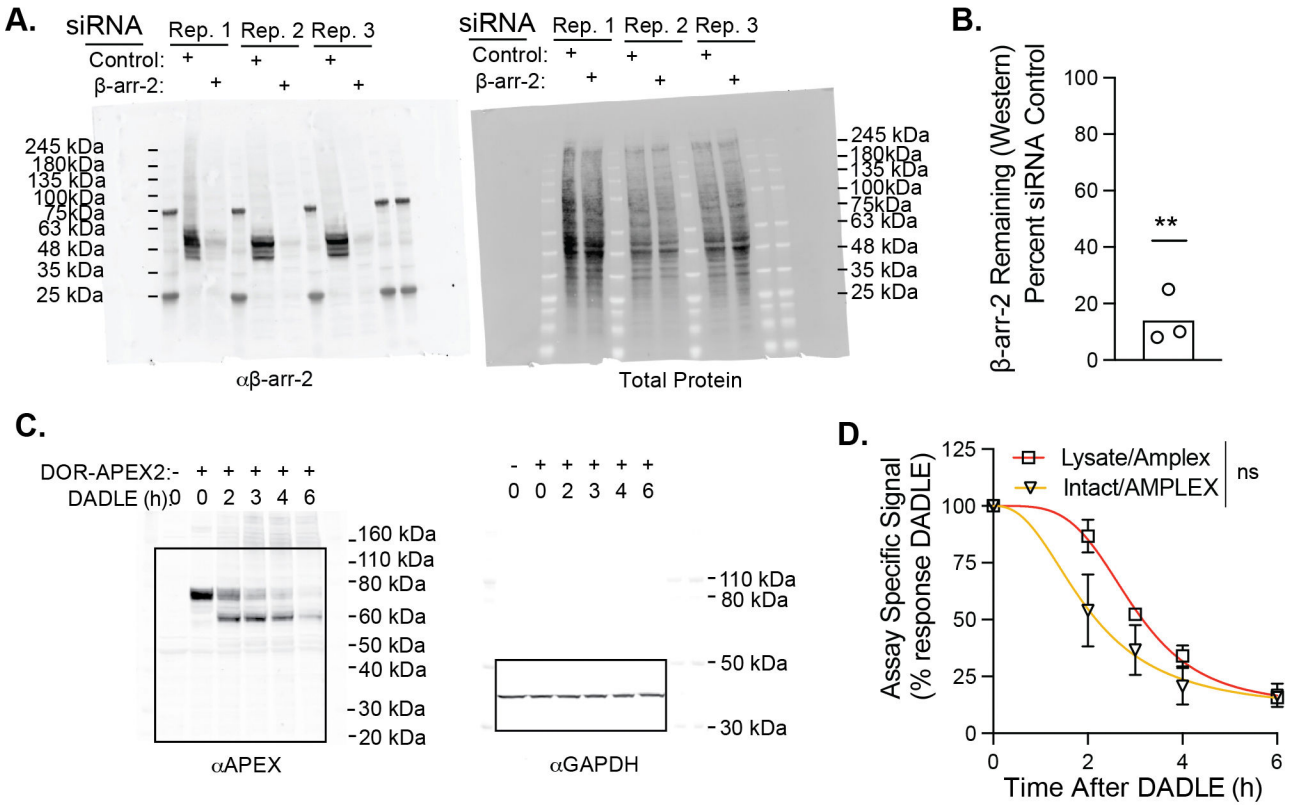

Extended Data Figure 3: APEX2-based fluorescence biosensor for GPCR downregulation.

(a) Uncropped western blots showing knockdown of β-arrestin-2 or total protein stain, N=3 independent experiments. (b) Quantification of β-arrestin-2 knockdown. N=3 independent experiments were analyzed with a one sample, two-tailed, t test (theoretical mean 100, p=0.0039).(c) Uncropped western blots corresponding to 1G showing APEX2 proteolysis or GAPDH loading control. (d). Comparison of signal loss from between lysate- or intact-

APEX2/AUR assay from HEK293 cells stably expressing CMV:DOR stimulated with 10 μM DADLE. N=3 independent experiments shown as mean ± SD, fit to a non-linear regression, and analyzed with a two-way ANOVA across the time-course (alpha=0.05, ns across time course and at all timepoints).

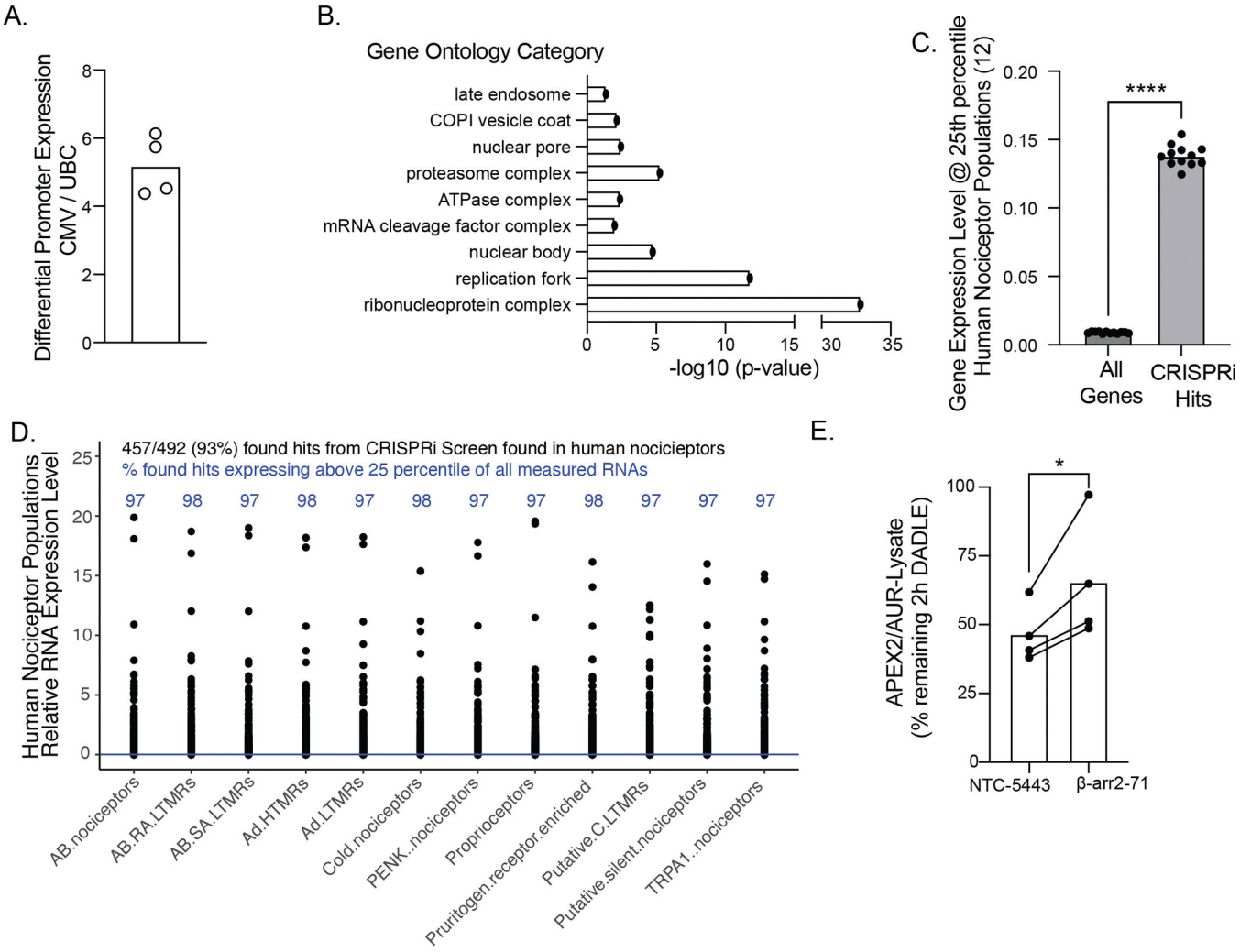

Extended Data Figure 4: Genome-wide CRISPRi screen for genes affecting DOR expression and trafficking.

(a) Relative surface expression of DOR-APEX2 stably expressed from the CMV or UBC promoter, probed with M1 anti-FLAG, and analyzed with a Beckman Coulter Cytoflex S, N=4 independent experiments. (b) Gene ontology overrepresentation test from the 492 hits from the CRISPRi screen analyzed using PANTHER analysis for “Slim Cellular Component” with a Fisher’s exact test with Bonferroni correction for multiple comparisons, and data plotted based on calculated p-value. (c) Relative RNA expression level of genes at the 25th percentile from 12 human nociceptor cell types examining all detected RNAs or CRISPRi hits. Relative expression level analyzed with a two-tailed paired t-test comparing all 12 cell types (p=3.02E-15). (d) Analysis of relative RNA expression of CRISPRi hits in a published dataset of 12 human nociceptor cell types. CRISPRi hits found shown in

black, 25th percentile of RNA expression level of the overall dataset shown with the blue line, and percent of CRISPRi hits above the bottom quartile noted in blue text. (e) Effects of β-arrestin-2 targeting sgRNA on DOR trafficking to the lysosome were analyzed in HEK293-FLP cells stably expressing UBC:DOR-APEX2 and dCas9-BFP-KRAB using the APEX/AUR lysate assay with no DADLE stimulation or 2 h DADLE (10 μM) stimulation, N=4 independent experiments, replicates connected by line. Data were analyzed using a two-tailed paired t-test (p=0.0485).

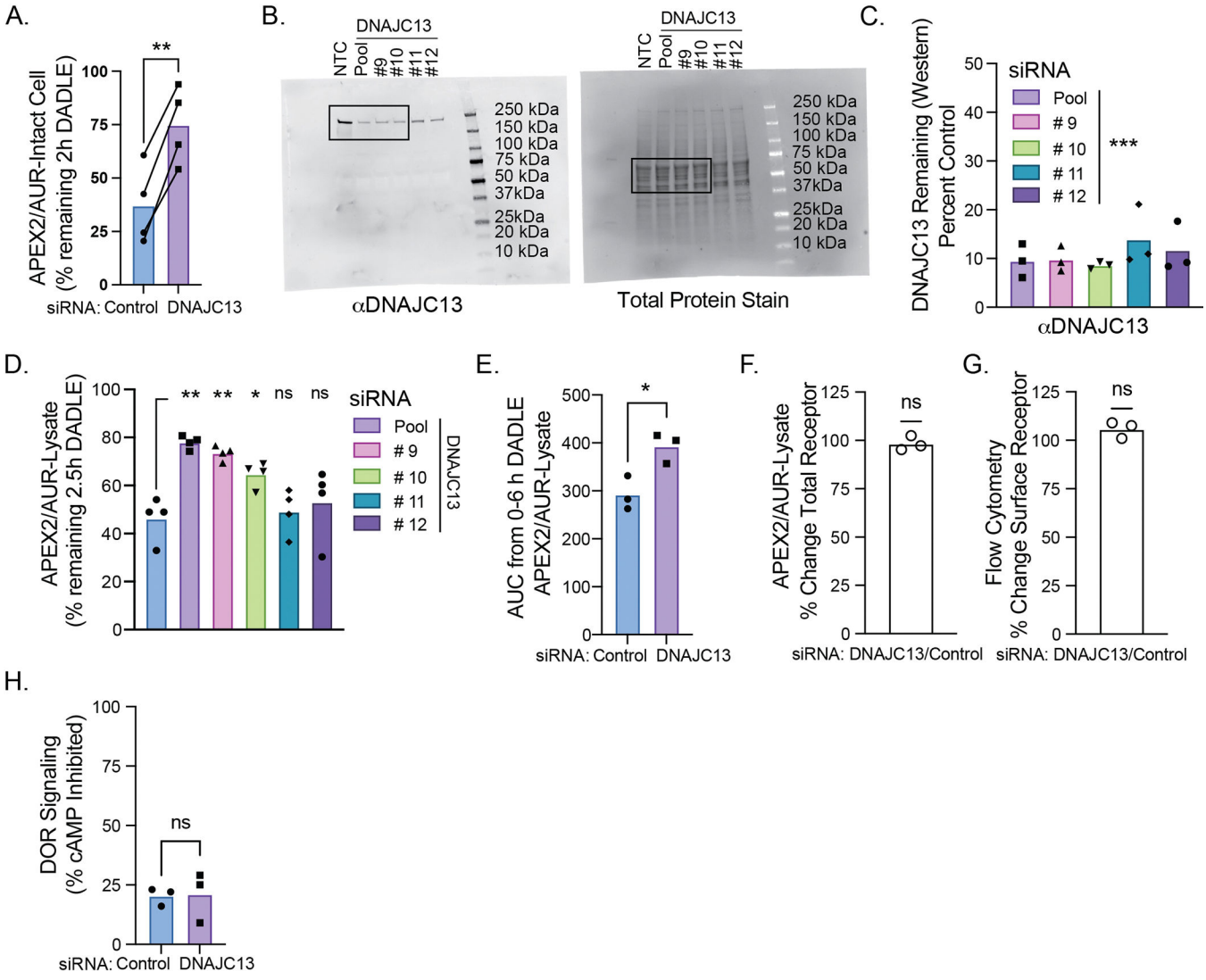

Extended Data Figure 5: DNAJC13 regulates trafficking of DOR to the lysosome.

(a) Single cell analysis of APEX2/AUR intact assay following knockdown of DNAJC13 and no DADLE treatment or 2 h stimulation with 10 μM DADLE. N=4 independent experiments connected by lines and analyzed using a two-tailed, paired t-test (p=0.002). (b) Uncropped western blot corresponding to Figure 3B. (c) Quantification of DNAJC13 knockdown as analyzed by western blot. N=3 independent experiments were analyzed using a paired one-way ANOVA (alpha: 0.05): p=0.0004. (d) APEX2/AUR lysate assay following siRNA

transfection with HEK293 cells stably expressing UBC:DOR-APEX2 with siRNA pool, or individual siRNAs, targeting DNAJC13 or a control. Cells had no DADLE treatment or 2.5 h stimulation with 10 μM DADLE. N=3 independent experiments were analyzed using a paired one-way ANOVA with Dunnett's multiple comparisons test (alpha: 0.05). Adjusted p-values vs control: pool (0.003), #9 (0.0015), #10 (0.0310). Data for pooled siRNA, #9, and #10 also shown in Figure 3C. (e) Area under the curve (AUC) analysis of Figure 3D. APEX2/AUR lysate assay time-course of 10 μM DADLE stimulation following siRNA transfection with HEK293 cells stably expressing UBC:DOR-APEX2. Cells were treated with 10 μM for 0 to 6 hours. N=3 independent experiments were analyzed with a two-tailed, paired t-test (0.0130). (f) Total DOR expression analyzed by the APEX2/AUR lysate assay comparing knockdown of DNAJC13 to control. N=3 independent experiments were analyzed with a one sample, two-tailed, t test (theoretical mean 100). (g) Surface DOR expression analyzed flow cytometry comparing knockdown of DNAJC13 to control. N=3 independent experiments were analyzed with a one sample, two-tailed, t test (theoretical mean 100). (h) DOR signaling following siRNA transfection with HEK293 cells stably expressing UBC:DOR-APEX2 with siRNA control or siRNA pool targeting DNAJC13. Cells were simultaneously treated with the agonist isoproterenol (30 nM) to stimulate the endogenous B2AR and the DOR agonist DADLE (10 μM). N=3 independent experiments were analyzed using a two-tailed paired t-test.

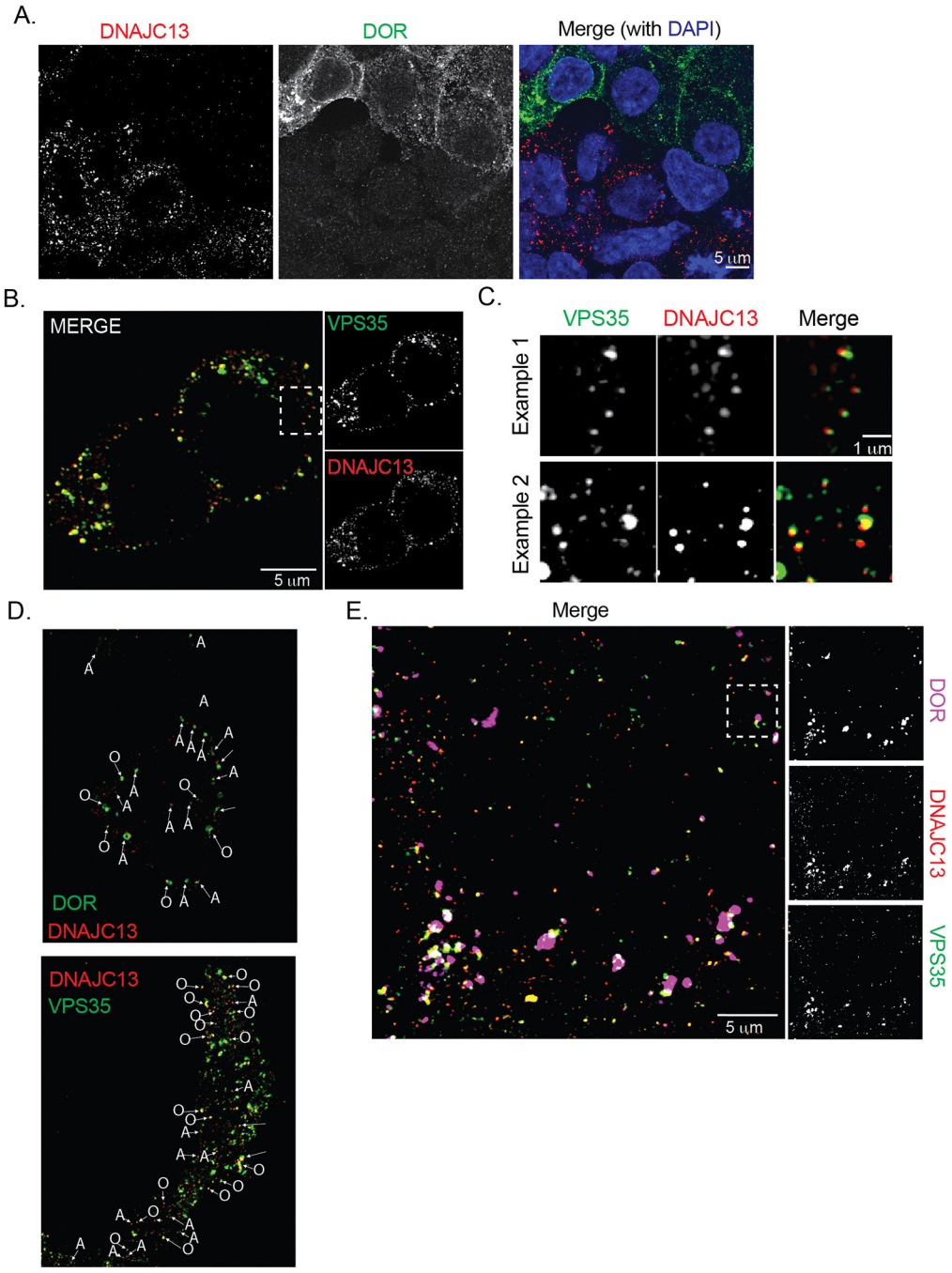

Extended Data Figure 6: DNAJC13 regulates trafficking of DOR to the lysosome.

(a) Validation of rabbit anti-DNAJC13 antibody using two populations of cells independently transfected with control siRNA (HEK293-FLP) or a siRNA pool targeting DNAJC13 (HEK293 FLP UBC:DOR-APEX2). Populations were mixed 48 h after transfection, fixed and permeabilized at 72 h, and then probed with anti-FLAG (DOR), anti-DNAJC13, and DAPI. Image is single confocal slice, scale bar is 5 µm, N=3 independent experiments. (b,c) Localization of DNAJC13 (anti-DNAJC13) and VPS35 (anti-VPS35) in HEK293-FLP cells stably expressing UBC:DOR-APEX2 were stimulated with 10 µM

DADLE for 15 min. Image is single confocal slice, scale bar 5 μm in (b) and 1 μm in (c). N=3 independent experiments, “Example 1” comes from white box in Extended Data 6B, and “Example 2” comes from an independent replicate. (d) Example of the adjacency scoring metric (A=adjacent, O=overlap). (e) Localization of DOR (anti-FLAG), DNAJC13 (anti-DNAJC13), and VPS35 (anti-VPS35) were analyzed in HEK293-FLP cells stably expressing UBC:DOR-APEX2 stimulated with 10 μM DADLE for 15 min. Image is single confocal slice corresponding to 4E example 1, scale bar 5 μm. N=3 independent experiments, representative example shown.

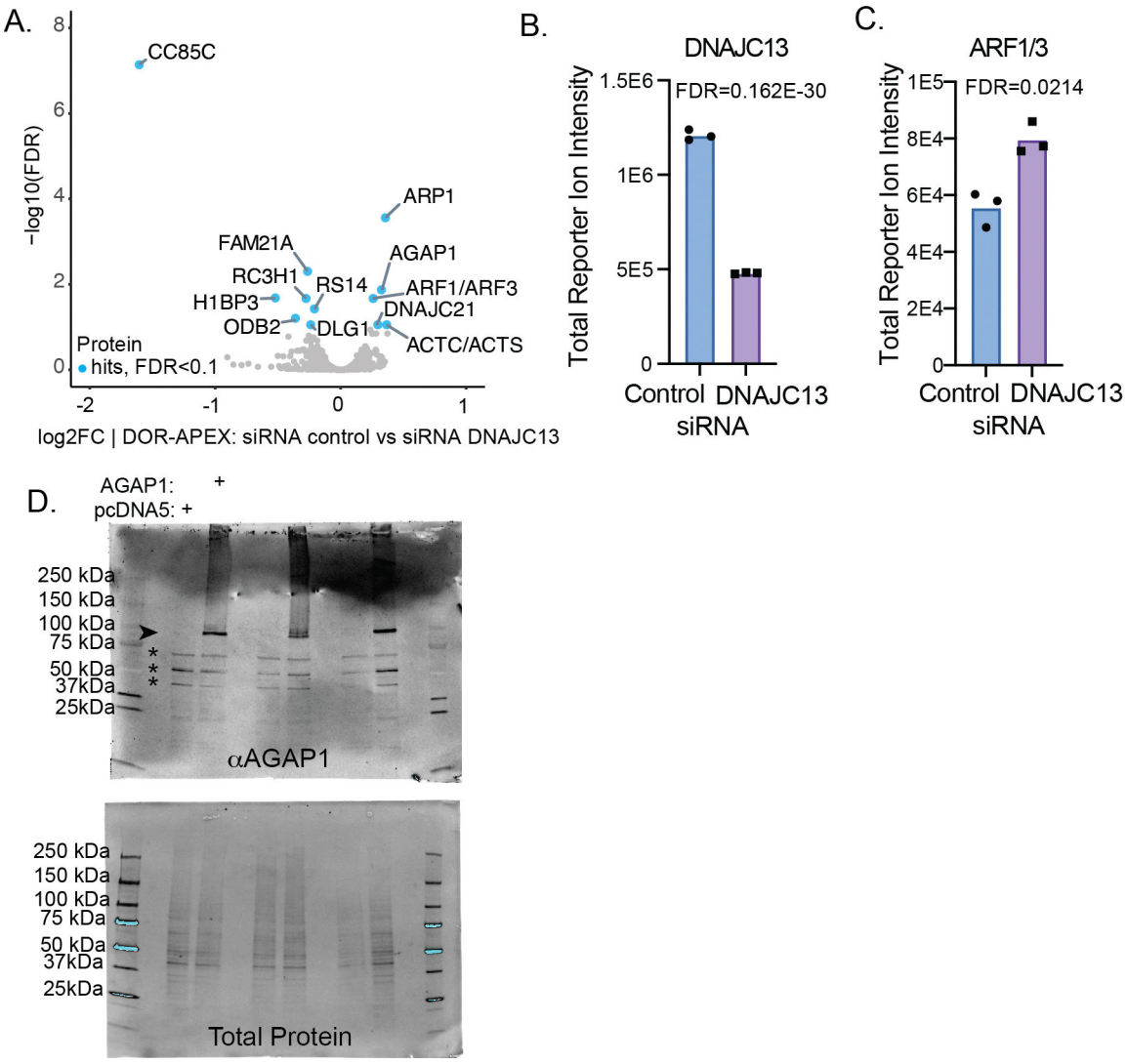

Extended Data Figure 7: Loss of DNAJC13 remodels the endosomal DOR proteome.

(a) Volcano plot of fold change (FC) comparing abundance of proteins following DOR-APEX2 mediated proximity labeling in cells transfected with siRNA control or siRNA pool targeting DNAJC13. N=3 independent experiments were analyzed using edgeR’s exact test with Benjamini-Hochberg correction for multiple comparisons. Proteins with an FDR <0.1 are denoted as hits (blue). For visualization, volcano plot is cropped and does not

show DNAJC13 (log2FC=−1.33; -log10(FDR)=29.8). (b,c) Total reporter ion intensity from TMT mass spectrometry from DOR-APEX2 proximity labeling in control cells or cells with DNAJC13 knockdown. N=3 independent experiments were analyzed using edgeR's exact test with Benjamini-Hochberg correction for multiple comparisons, control vs DNAJC13 (DNAJC13: FDR= 0.162E-30; ARF1/3: FDR=0.0214). (d) Overexpression of AGAP1 analyzed by western blot. AGAP1 band marked with an arrow, non-specific bands marked with stars, total protein stain was used as the loading control, N=3 independent experiments shown.

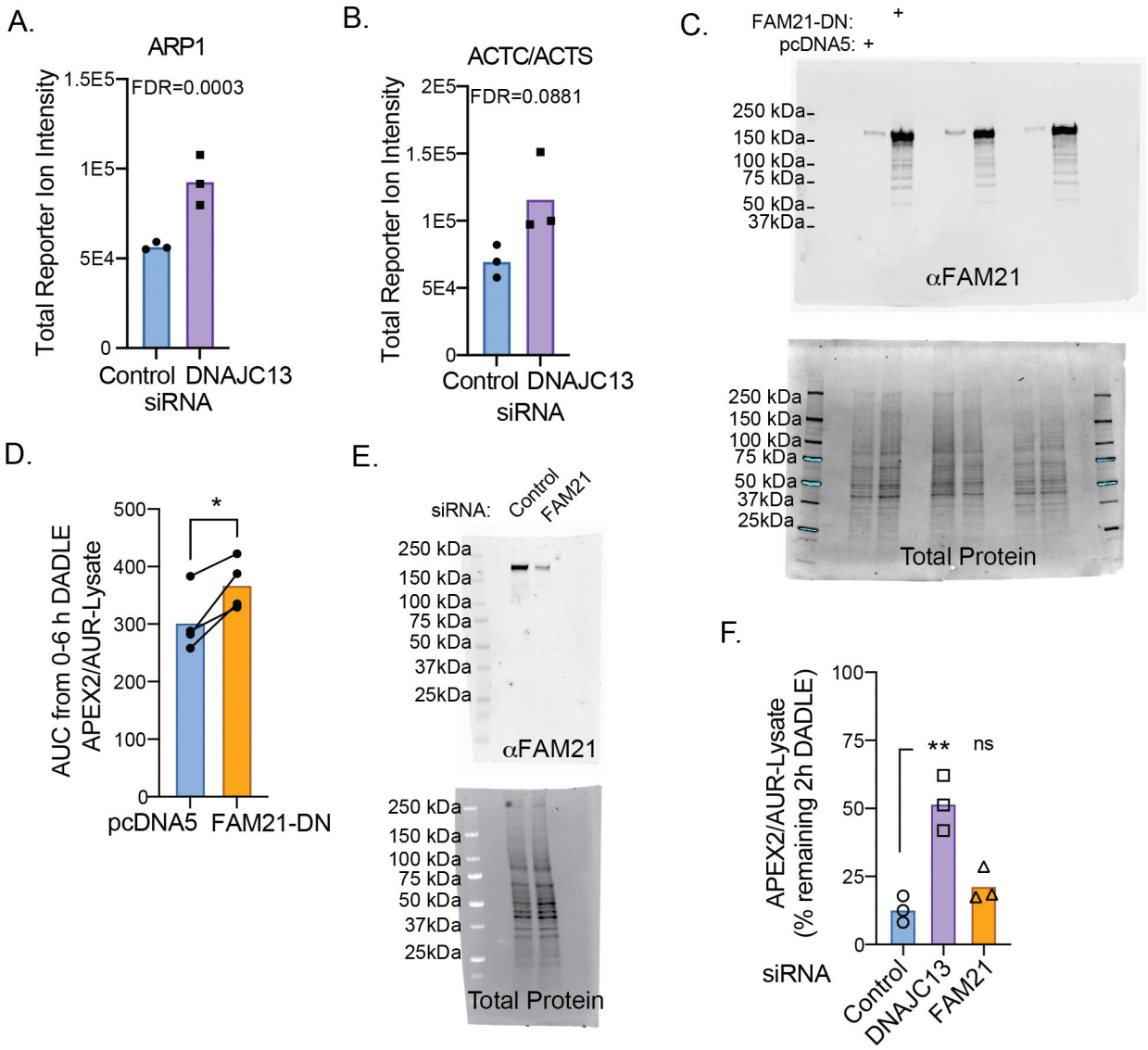

Extended Data Figure 8: Loss of DNAJC13 remodels the endosomal DOR proteome.
(a,b) Total reporter ion intensity from TMT mass spectrometry from DOR-APEX2 proximity labeling in control cells or cells with DNAJC13 knockdown. N=3 independent experiments were analyzed using edgeR's exact test with Benjamini-Hochberg correction for multiple comparisons, control vs DNAJC13 (ARP1: FDR= 0.0003; ARF1/3:

FDR=0.0881). (c) Overexpression of dominant negative FAM21 (FAM21-DN) analyzed by western blot. Total protein stain was used as the loading control, N=3 independent experiments shown. (d) Area under the curve (AUC) analysis from APEX2/AUR lysate assay time course from 0–6 hours following 10 μM DADLE stimulation in HEK293 cells stably expressing UBC:DOR-APEX2 and transiently expressing empty vector or FAM21-DN. N=4 independent experiments were connected by lines and analyzed with a two-tailed, paired t-test (FAM21-DN: p=0.0258). (e) Western blots showing knockdown of FAM21 detected in HEK293-FLP cells stably expressing UBC:DOR-APEX2 by western blot 72 h after siRNA transfection. Total protein stain was used as the loading control, N=3 independent experiments, representative example shown. (f) APEX2/AUR lysate assay following siRNA transfection with HEK293 cells stably expressing UBC:DOR-APEX2 with siRNA control or siRNA pools targeting DNAJC13 or FAM21A/C. Cells had no DADLE treatment or 2 h stimulation with 10 μM DADLE. N=3 independent experiments were analyzed using a paired one-way ANOVA (alpha: 0.05) with Dunnett's multiple comparisons test. Adjusted p-values when compared to NTC: DNAJC13 (0.0352), FAM21 (0.2886).

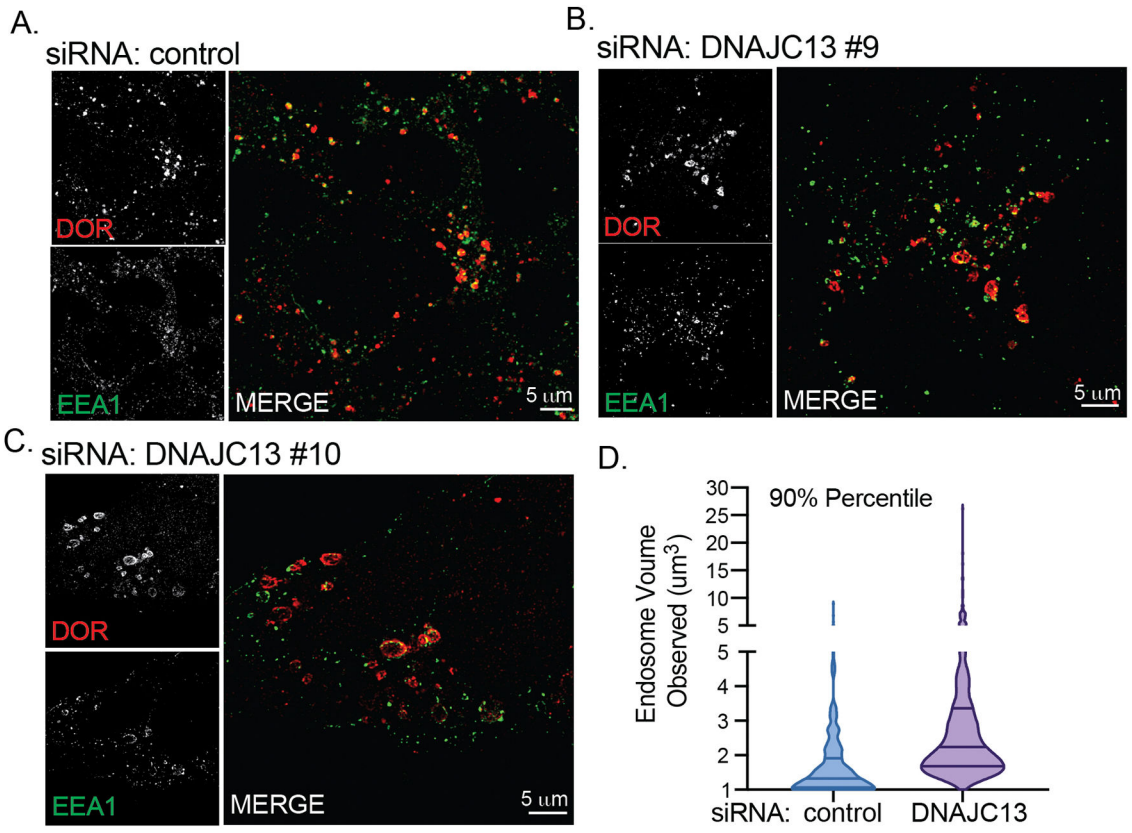

Extended Data Figure 9: DNAJC13 knockdown causes expansion of DOR endosomes.

(a-c) Fixed and permeabilized HEK293-FLP cells stably expressing UBC:DOR-APEX2 were probed to detect endosomes (anti-EEA1) containing DOR (anti-APEX). Cells were treated with individual siRNAs targeting DNAJC13 or siRNA control for 72 h prior to stimulated with 10 μM DADLE for 15 min. Scale bar 5 μm. N=3 independent

experiments, representative example shown. (d) Volume of DOR- and EEA1-positive endosomes measured following knockdown of DNAJC13. Data corresponding to top 10% (90th percentile) of Figure 6D, data from N=3 independent experiments.

Supplementary Material

Refer to Web version on PubMed Central for supplementary material.

Acknowledgements

We thank Mark von Zastrow for essential advice, feedback on this manuscript, and support of early studies contributing to this work. We thank R. Sarah Elmes (UCSF, CA) for critical advice and assistance with flow cytometry. We thank the OHSU Proteomics Shared Resource core for assistance with TMT-labeling, mass spectrometry, and proteomics data analysis.

Funding and Additional information.

This work was supported by the National Institute of Health (GM137835 and DA043607 to BL, NS127847 to NGT, AG062359 to MK). BL is also supported by OHSU startup funds. Early studies contributing to this work were supported by Mark von Zastrow at UCSF (DA010711 and DA012864). This work was carried out with help of core facility resources: the OHSU Flow Cytometry Core (Matthew Schleisman and Pamela Canaday), the OHSU Advanced Light Microscopy Core (Brian Jenkins and Stefanie Kaech Petrie), the OHSU Proteomics Shared Resource Core (Ashok Reddy and Phillip Wilmarth; supported by the National Institutes of Health under award P30EY010572, P30CA069533, S10OD012246), the UCSF Center for Advanced Technology (Eric Chow), and the UCSF Helen Diller Family Comprehensive Cancer Center Laboratory for Cell Analysis (R. Sarah Elmes; supported by the National Institutes of Health under award P30CA082103).

Data Availability

All data generated and analyzed in this study are included as figures, extended data or supplementary tables, or source data. The nociceptor dataset was download from: https://sensoryomics.shinyapps.io/RNA-Data/. The human proteome was downloaded from the uniprot human protein database: https://www.uniprot.org/proteomes/UP000005640. RAW proteomics data have been deposited to the ProteomeXchange Consortium via the PRIDE partner repository with the dataset identifier: PXD044921. Data from the genome wide CRISPRi screen were deposited to the Gene Expression Omnibus (GEO) with the dataset identifier: GSE242366

References

1. Hanyaloglu AC & von Zastrow M Regulation of GPCRs by endocytic membrane trafficking and its potential implications. Annu. Rev. Pharmacol. Toxicol. 48, 537–568 (2008). [PubMed: 18184106]
2. Irannejad R & Lobingier BT GPCRs at endosomes: Sorting, signaling, and recycling. GPCRs as Therapeutic Targets 180–196 Preprint at 10.1002/9781119564782.ch6 (2022).
3. Gilbert LA et al. Genome-scale CRISPR-mediated control of gene repression and activation. Cell 159, 647–661 (2014). [PubMed: 25307932]
4. Doench JG Am I ready for CRISPR? A user's guide to genetic screens. Nat. Rev. Genet. 19, 67–80 (2018). [PubMed: 29199283]
5. Law PY, Hom DS & Loh HH Down-regulation of opiate receptor in neuroblastoma × glioma NG108–15 hybrid cells. Chloroquine promotes accumulation of tritiated enkephalin in the lysosomes. J. Biol. Chem. 259, 4096–4104 (1984). [PubMed: 6323457]
6. Hislop JN, Henry AG, Marchese A & von Zastrow M Ubiquitination regulates proteolytic processing of G protein-coupled receptors after their sorting to lysosomes. J. Biol. Chem. 284, 19361–19370 (2009). [PubMed: 19433584]

7. Poole DP et al. Localization and regulation of fluorescently labeled delta opioid receptor, expressed in Enteric neurons of mice. Gastroenterology 141, 982–991.e8 (2011). [PubMed: 21699782]
8. Lam SS et al. Directed evolution of APEX2 for electron microscopy and proximity labeling. Nat. Methods 12, 51–54 (2015). [PubMed: 25419960]
9. Lobingier BT et al. An Approach to Spatiotemporally Resolve Protein Interaction Networks in Living Cells. Cell 169, 350–360.e12 (2017). [PubMed: 28388416]
10. Civciristov S et al. Ligand-dependent spatiotemporal signaling profiles of the μ-opioid receptor are controlled by distinct protein-interaction networks. J. Biol. Chem. 294, 16198–16213 (2019). [PubMed: 31515267]
11. Polacco BJ et al. Profiling the proximal proteome of the activated μ-opioid receptor. Nat. Chem. Biol. (2024) doi:10.1038/s41589-024-01588-3.
12. Pradhan AA, Befort K, Nozaki C, Gavériaux-Ruff C & Kieffer BL The delta opioid receptor: an evolving target for the treatment of brain disorders. Trends Pharmacol. Sci. 32, 581–590 (2011). [PubMed: 21925742]
13. Quirion B, Bergeron F, Blais V & Gendron L The delta-opioid receptor; A target for the treatment of pain. Front. Mol. Neurosci. 13, 52 (2020). [PubMed: 32431594]
14. St-Louis É et al. Involvement of the coatomer protein complex I in the intracellular traffic of the delta opioid receptor. Mol. Cell. Neurosci. 79, 53–63 (2017). [PubMed: 28041939]
15. Shiwarski DJ, Crilly SE, Dates A & Puthenveedu MA Dual RXR motifs regulate nerve growth factor-mediated intracellular retention of the delta opioid receptor. Mol. Biol. Cell 30, 680–690 (2019). [PubMed: 30601694]
16. Gendron L, Cahill CM, von Zastrow M, Schiller PW & Pineyro G Molecular pharmacology of δ-opioid receptors. Pharmacol. Rev. 68, 631–700 (2016). [PubMed: 27343248]
17. Whistler JL et al. Modulation of postendocytic sorting of G protein-coupled receptors. Science 297, 615–620 (2002). [PubMed: 12142540]
18. Scherrer G et al. Knockin mice expressing fluorescent delta-opioid receptors uncover G protein-coupled receptor dynamics in vivo. Proc. Natl. Acad. Sci. U. S. A. 103, 9691–9696 (2006). [PubMed: 16766653]
19. Wittrup KD & Bailey JE A single-cell assay of beta-galactosidase activity in Saccharomyces cerevisiae. Cytometry 9, 394–404 (1988). [PubMed: 3135986]
20. Ryder AG, Power S & Glynn TJ Fluorescence-lifetime-based pH sensing using resorufin. in Opto-Ireland 2002: Optics and Photonics Technologies and Applications (ed. Glynn TJ) (SPIE, 2003). doi:10.1117/12.463983.
21. Towne V, Will M, Oswald B & Zhao Q Complexities in horseradish peroxidase-catalyzed oxidation of dihydroxyphenoxazine derivatives: appropriate ranges for pH values and hydrogen peroxide concentrations in quantitative analysis. Anal. Biochem. 334, 290–296 (2004). [PubMed: 15494136]
22. Zhang X, Wang F, Chen X, Chen Y & Ma L Post-endocytic fates of delta-opioid receptor are regulated by GRK2-mediated receptor phosphorylation and distinct beta-arrestin isoforms. J. Neurochem. 106, 781–792 (2008). [PubMed: 18419762]
23. Tian R et al. CRISPR interference-based platform for multimodal genetic screens in human iPSC-derived neurons. Neuron 104, 239–255.e12 (2019). [PubMed: 31422865]
24. McGilvray PT et al. An ER translocon for multi-pass membrane protein biogenesis. Elife 9, (2020).
25. Tavares-Ferreira D et al. Spatial transcriptomics of dorsal root ganglia identifies molecular signatures of human nociceptors. Sci. Transl. Med. 14, eabj8186 (2022). [PubMed: 35171654]
26. Hislop JN, Marley A & von Zastrow M Role of mammalian vacuolar protein-sorting proteins in endocytic trafficking of a non-ubiquitinated G protein-coupled receptor to lysosomes. J. Biol. Chem. 279, 22522–22531 (2004). [PubMed: 15024011]
27. Liu P, Khvotchev M, Li YC, Chanaday NL & Kavalali ET Copine-6 binds to SNAREs and selectively suppresses spontaneous neurotransmission. J. Neurosci. 38, 5888–5899 (2018). [PubMed: 29802203]
28. Hermle T et al. GAPVD1 and ANKFY1 mutations implicate RAB5 regulation in nephrotic syndrome. J. Am. Soc. Nephrol. 29, 2123–2138 (2018). [PubMed: 29959197]

29. Lacey J et al. Sorting Nexin 24 is required for α-granule biogenesis and cargo delivery in megakaryocytes. Haematologica (2022) doi:10.3324/haematol.2021.279636.
30. Fujibayashi A et al. Human RME-8 is involved in membrane trafficking through early endosomes. Cell Struct. Funct. 33, 35–50 (2008). [PubMed: 18256511]
31. Liu K et al. WDR91 is a Rab7 effector required for neuronal development. J. Cell Biol. 216, 3307–3321 (2017). [PubMed: 28860274]
32. Zhang Y, Grant B & Hirsh D RME-8, a conserved J-domain protein, is required for endocytosis in Caenorhabditis elegans. Mol. Biol. Cell 12, 2011–2021 (2001). [PubMed: 11451999]
33. Girard M, Poupon V, Blondeau F & McPherson PS The DnaJ-domain protein RME-8 functions in endosomal trafficking. J. Biol. Chem. 280, 40135–40143 (2005). [PubMed: 16179350]
34. Popoff V et al. Analysis of articulation between clathrin and retromer in retrograde sorting on early endosomes. Traffic 10, 1868–1880 (2009). [PubMed: 19874558]
35. Shi A et al. Regulation of endosomal clathrin and retromer-mediated endosome to Golgi retrograde transport by the J-domain protein RME-8. EMBO J. 28, 3290–3302 (2009). [PubMed: 19763082]
36. Xhabija B & Vacratsis PO Receptor-mediated endocytosis 8 utilizes an N-terminal phosphoinositide-binding motif to regulate endosomal clathrin dynamics. J. Biol. Chem. 290, 21676–21689 (2015). [PubMed: 26134565]
37. Freeman CL, Hesketh G & Seaman MNJ RME-8 coordinates the activity of the WASH complex with the function of the retromer SNX dimer to control endosomal tubulation. J. Cell Sci. 127, 2053–2070 (2014). [PubMed: 24643499]
38. Norris A et al. SNX-1 and RME-8 oppose the assembly of HGRS-1/ESCRT-0 degradative microdomains on endosomes. Proc. Natl. Acad. Sci. U. S. A. 114, E307–E316 (2017). [PubMed: 28053230]
39. Girard M & McPherson PS RME-8 regulates trafficking of the epidermal growth factor receptor. FEBS Lett. 582, 961–966 (2008). [PubMed: 18307993]
40. Puthenveedu MA et al. Sequence-dependent sorting of recycling proteins by actin-stabilized endosomal microdomains. Cell 143, 761–773 (2010). [PubMed: 21111236]
41. Varandas KC, Irannejad R & von Zastrow M Retromer endosome exit domains serve multiple trafficking destinations and regulate local G protein activation by GPCRs. Curr. Biol. 26, 3129–3142 (2016). [PubMed: 27839977]
42. Cullen PJ & Steinberg F To degrade or not to degrade: mechanisms and significance of endocytic recycling. Nat. Rev. Mol. Cell Biol. 19, 679–696 (2018). [PubMed: 30194414]
43. Norris A, McManus CT, Wang S, Ying R & Grant BD Mutagenesis and structural modeling implicate RME-8 IWN domains as conformational control points. PLoS Genet. 18, e1010296 (2022). [PubMed: 36279308]
44. Nie Z et al. AGAP1, an endosome-associated, phosphoinositide-dependent ADP-ribosylation factor GTPase-activating protein that affects actin cytoskeleton. J. Biol. Chem. 277, 48965–48975 (2002). [PubMed: 12388557]
45. Nie Z et al. Specific regulation of the adaptor protein complex AP-3 by the Arf GAP AGAP1. Dev. Cell 5, 513–521 (2003). [PubMed: 12967569]
46. Arnold M et al. The endosome localized arf-GAP AGAP1 modulates dendritic spine morphology downstream of the neurodevelopmental disorder factor dysbindin. Front. Cell. Neurosci. 10, 218 (2016). [PubMed: 27713690]
47. Derivery E et al. The Arp2/3 activator WASH controls the fission of endosomes through a large multiprotein complex. Dev. Cell 17, 712–723 (2009). [PubMed: 19922875]
48. Duleh SN & Welch MD WASH and the Arp2/3 complex regulate endosome shape and trafficking. Cytoskeleton (Hoboken) 67, 193–206 (2010). [PubMed: 20175130]
49. Gomez TS, Gorman JA, de Narvajas AA-M, Koenig AO & Billadeau DD Trafficking defects in WASH-knockout fibroblasts originate from collapsed endosomal and lysosomal networks. Mol. Biol. Cell 23, 3215–3228 (2012). [PubMed: 22718907]
50. Piotrowski JT, Gomez TS, Schoon RA, Mangalam AK & Billadeau DD WASH knockout T cells demonstrate defective receptor trafficking, proliferation, and effector function. Mol. Cell. Biol. 33, 958–973 (2013). [PubMed: 23275443]

51. Fokin AI et al. The Arp1/11 minifilament of dynactin primes the endosomal Arp2/3 complex. Sci. Adv. 7, (2021).
52. Jia D, Gomez TS, Billadeau DD & Rosen MK Multiple repeat elements within the FAM21 tail link the WASH actin regulatory complex to the retromer. Mol. Biol. Cell 23, 2352–2361 (2012). [PubMed: 22513087]
53. Harbour ME, Breusegem SY & Seaman MNJ Recruitment of the endosomal WASH complex is mediated by the extended “tail” of Fam21 binding to the retromer protein Vps35. Biochem. J. 442, 209–220 (2012). [PubMed: 22070227]
54. Helfer E et al. Endosomal recruitment of the WASH complex: active sequences and mutations impairing interaction with the retromer. Biol. Cell 105, 191–207 (2013). [PubMed: 23331060]
55. Dostál V, Humhalová T, Beránková P, Pácalt O & Libusová L SWIP mediates retromer-independent membrane recruitment of the WASH complex. Traffic 24, 216–230 (2023). [PubMed: 36995008]
56. Katayama H, Yamamoto A, Mizushima N, Yoshimori T & Miyawaki A GFP-like proteins stably accumulate in lysosomes. Cell Struct. Funct. 33, 1–12 (2008). [PubMed: 18256512]
57. Ni H-M et al. Dissecting the dynamic turnover of GFP-LC3 in the autolysosome. Autophagy 7, 188–204 (2011). [PubMed: 21107021]
58. Kim S, Choi S & Kang D Quantitative and qualitative analysis of autophagy flux using imaging. BMB Rep. 53, 241–247 (2020). [PubMed: 32317089]
59. Pradhan AAA et al. In vivo delta opioid receptor internalization controls behavioral effects of agonists. PLoS One 4, e5425 (2009). [PubMed: 19412545]
60. Pradhan AAA et al. Ligand-directed trafficking of the δ-opioid receptor in vivo: two paths toward analgesic tolerance. J. Neurosci. 30, 16459–16468 (2010). [PubMed: 21147985]
61. DiCello JJ et al. Agonist-dependent development of delta opioid receptor tolerance in the colon. Cell. Mol. Life Sci. 76, 3033–3050 (2019). [PubMed: 30904952]
62. Vicente-Sanchez A et al. Tolerance to high-internalizing δ opioid receptor agonist is critically mediated by arrestin 2. Br. J. Pharmacol. 175, 3050–3059 (2018). [PubMed: 29722902]
63. Gomez-Lamarca M, Snowdon LA, Seib E, Klein T & Bray S Rme-8 depletion perturbs Notch recycling and predisposes to pathogenic signaling. J. Cell Biol. 210, 517–517 (2015). [PubMed: 26240186]

Methods Only References

64. Peng GE, Pessino V, Huang B & von Zastrow M Spatial decoding of endosomal cAMP signals by a metastable cytoplasmic PKA network. Nat. Chem. Biol. 17, 558–566 (2021). [PubMed: 33649598]
65. Gilbert LA et al. CRISPR-mediated modular RNA-guided regulation of transcription in eukaryotes. Cell 154, 442–451 (2013). [PubMed: 23849981]
66. Horlbeck MA et al. Compact and highly active next-generation libraries for CRISPR-mediated gene repression and activation. Elife 5, (2016).
67. Kampmann M, Bassik MC & Weissman JS Functional genomics platform for pooled screening and generation of mammalian genetic interaction maps. Nat. Protoc. 9, 1825–1847 (2014). [PubMed: 24992097]
68. Semesta K, Tian R, Kampmann M, Zastrow M & Tsvetanova N A high-throughput CRISPR interference screen for dissecting functional regulators of GPCR/cAMP signaling. FASEB J. 35, (2021).
69. Wilmarth PA, Riviere MA & David LL Techniques for accurate protein identification in shotgun proteomic studies of human, mouse, bovine, and chicken lenses. J. Ocul. Biol. Dis. Infor. 2, 223–234 (2009). [PubMed: 20157357]
70. Eng JK, Jahan TA & Hoopmann MR Comet: an open-source MS/MS sequence database search tool. Proteomics 13, 22–24 (2013). [PubMed: 23148064]
71. Elias JE & Gygi SP Target-decoy search strategy for increased confidence in large-scale protein identifications by mass spectrometry. Nat. Methods 4, 207–214 (2007). [PubMed: 17327847]

72. Robinson MD, McCarthy DJ & Smyth GK edgeR: a Bioconductor package for differential expression analysis of digital gene expression data. Bioinformatics 26, 139–140 (2010). [PubMed: 19910308]

73. Robinson MD & Oshlack A A scaling normalization method for differential expression analysis of RNA-seq data. Genome Biol. 11, R25 (2010) [PubMed: 20196867]

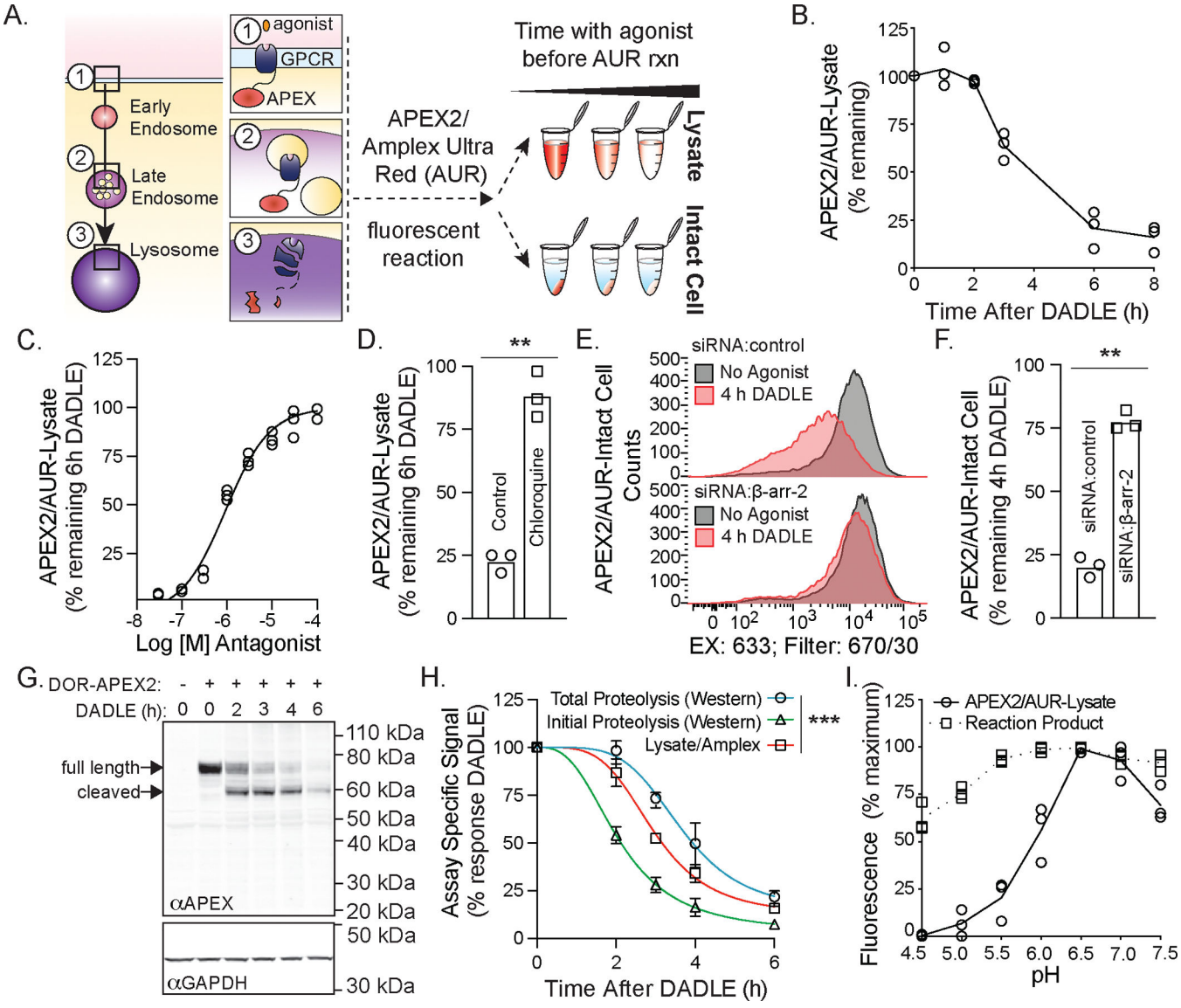

Fig. 1: APEX2-based fluorescence biosensor for GPCR downregulation

(a) GPCR-APEX2 and Amplex UltraRed (AUR) method

(b) Agonist-mediated signal loss in the APEX2/AUR lysate assay. HEK293 cells stably expressing CMV:DOR-APEX2 were stimulated with 10 μM DADLE for the indicated duration before the AUR reaction, data normalized to no agonist treatment, N=3 independent experiments.

(c) HEK293-FLP cells stably expressing UBC:DOR-APEX2 were treated simultaneously with DADLE (30 nM) and the antagonist naloxone (indicated concentration) for 6h before the AUR reaction and normalized to maximum fluorescence, N=2 (30 nM, 300 nM, 100 μM) or 3 (all other concentrations) independent experiments.

(d) Chloroquine pretreatment of HEK293 cells stably expressing CMV:DOR-APEX2 followed by 6 h stimulation with 10 μM DADLE before the APEX2/AUR lysate assay, data normalized to no agonist treatment. N=3 independent experiments were analyzed with a two-tailed, paired t-test (p=0.0068).

(e,f) Single cell analysis of APEX2/AUR intact assay after β-arrestin-2 knockdown and 4 h stimulation with DADLE (10 μM), and representative example shown in (e) and in (f) median fluorescence from N=3 independent replicates analyzed with a two-tailed, paired t-test (p=0.0031). Cells analyzed in (e): 21827 (control/no agonist), 21558 (control/agonist), 22601 (siRNA-β-arrestin-2/no agonist), 22363 (siRNA-β-arrestin-2/agonist).
(g) Proteolysis of APEX2-tagged DOR detected by western blot following DADLE treatment (10 μM) of HEK293 cells stably expressing CMV:DOR-APEX2, N=3 independent experiments, representative example shown.
(h) Quantification of western blot compared to APEX/AUR lysate assay. HEK293 cells stably expressing CMV:DOR-APEX2 were stimulated with 10 μM DADLE. N=3 independent experiments shown as mean ± SD, fit to a non-linear regression, and analyzed with a two-way ANOVA (alpha=0.05, p=0.0002, variation between assays) and Tukey's multiple comparisons comparing initial proteolysis (western) vs lysate amplex (2 h: p=0.0018; 3 h: p=0.0053, 4 h: p=0.0210; 6 h: p=0.0108) or total proteolysis (western) vs lysate amplex (3 h:p=0.0083).
(i) APEX2/AUR lysate assay (solid line) performed over pH range in a universal buffer. Reaction product (dotted line) denotes data in which the assay was performed at standard pH of 7.4 and then diluted into universal buffer at the noted pH. Data were normalized to the maximum fluorescence (pH 6.5), N=3 independent experiments.

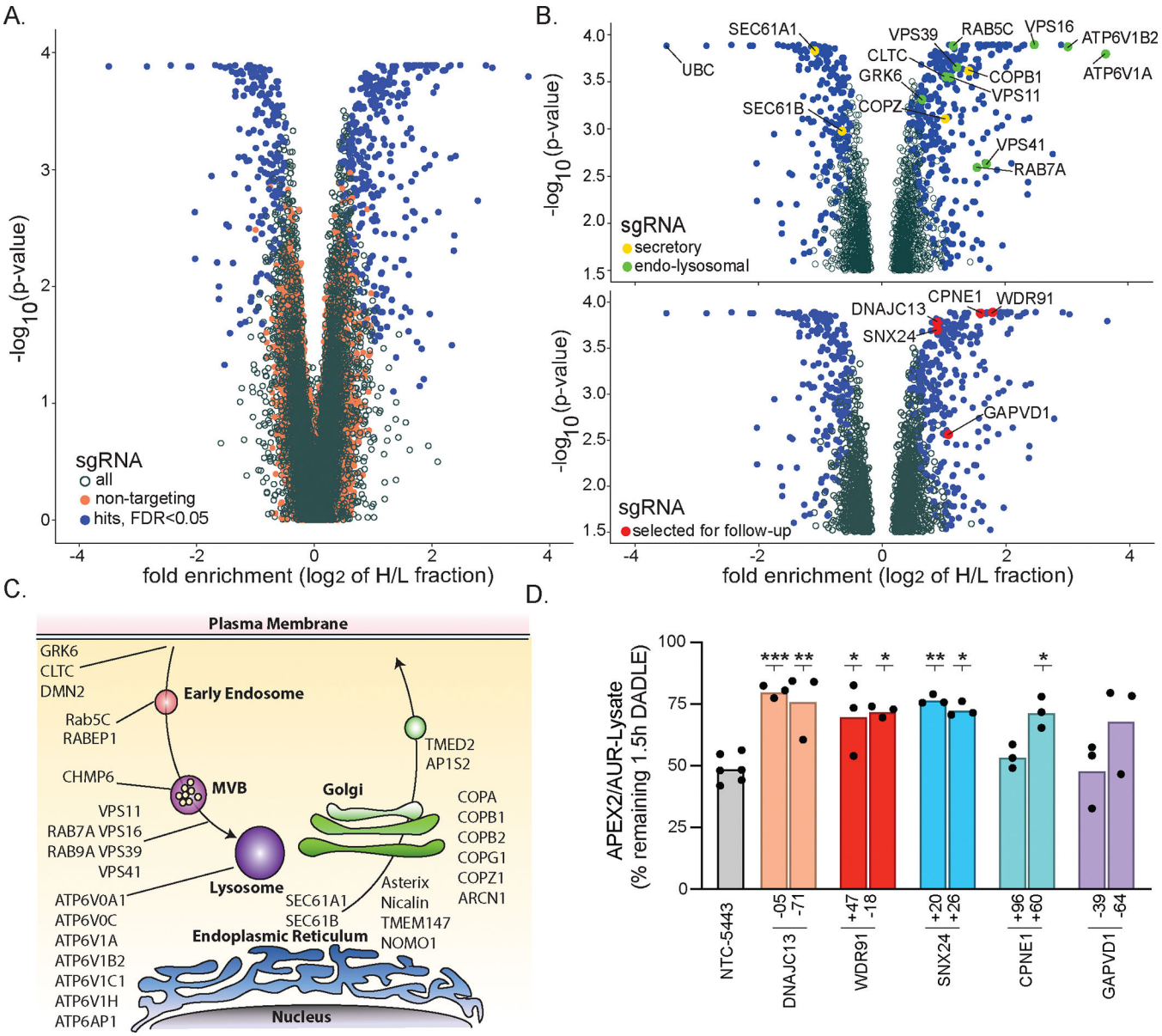

Fig. 2: Genome-wide CRISPRi screen for genes affecting DOR expression and trafficking.

(a-c) (a) Volcano plot of relative gene enrichment in the high (H) and low (L) signal sorted populations from all seven sub-libraries between FACS sorted bottom and top quartiles following APEX2/AUR intact cell reaction. Relative sgRNA enrichment between the populations was analyzed with a Mann-Whitney U test from N=1 independent experiment. Gene-targeting sgRNAs with an FDR <0.05 are denoted as hits (blue), non-targeting control sgRNAs (orange), and all other gene-targeting sgRNAs (open circles). (b) A subset of hits known to function in secretory or endo-lysosomal pathways are highlighted (upper) and hits selected for follow-up (lower). (c) A more comprehensive list of hits known to function in trafficking are diagramed based on primary known location of function.

(d) HEK293-FLP cells stably expressing UBC:DOR-APEX2, dCas9-BFP-KRAB, and the noted sgRNA, were analyzed using the APEX2/AUR lysate assay with no DADLE treatment

or 1.5 h stimulation with 10 μM DADLE. N=3 independent experiments for all TSS-targeting sgRNAs and N=6 independent experiments for the NTC. Data were analyzed using an unpaired one-way ANOVA (alpha: 0.05) with Dunnett's multiple comparisons test. Adjusted p-values when compared to NTC-5433: DNAJC13–05 (0.0008), DNAJC13–71 (0.0032), WDR96+47 (0.0329), WDR96–18 (0.0153), SNX24+20 (0.0027), SNX24+26 (0.0123), CPNE+60 (0.0181).

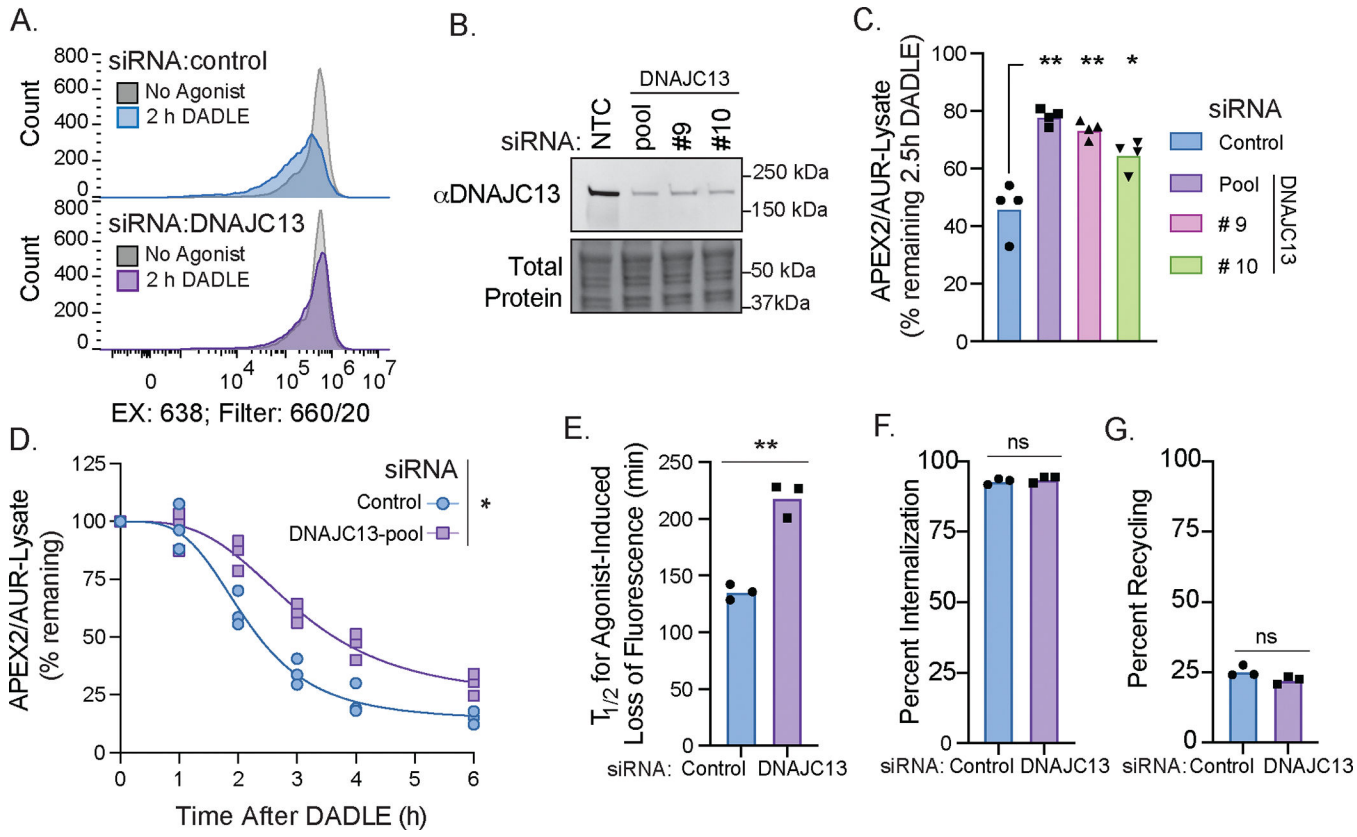

Figure 3: DNAJC13 regulates DOR trafficking to the lysosome.

(a) Single cell analysis of APEX2/AUR intact assay following knockdown of DNAJC13 and no DADLE treatment or 2 h stimulation with 10 μM DADLE. The fluorescent reaction product in HEK293-FLP cells stably expressing UBC:DOR-APEX2 was detected with a Beckman Coulter Cytoflex S, representative example shown (cells analyzed: 14935 (control) or 14960 (control+DADLE), 14764 (DNAJC13), 14902 (DNAJC13+DADLE)) and summary data from N=4 independent experiments plotted in Extended Data Fig. 5A.

(b) Knockdown of DNAJC13 in HEK293-FLP cells transfected with siRNA control, siRNA pool targeting DNAJC13, or individual siRNAs targeting DNAJC13 was analyzed by western blot. Total protein stain was used as the loading control, N=3 independent experiments, representative example shown, uncropped blots in Extended Data Fig. 5B.

(c) APEX2/AUR lysate assay following siRNA transfection with HEK293 cells stably expressing UBC:DOR-APEX2 with siRNA control, siRNA pool targeting DNAJC13, or individual siRNAs targeting DNAJC13. Cells had no DADLE treatment or 2.5 h stimulation with 10 μM DADLE. N=3 independent experiments were analyzed using a paired one-way ANOVA with Dunnett's multiple comparisons (alpha: 0.05). Adjusted p-values vs control: pool (0.0091), 9 (0.0468), 10 (0.0076).

(d) APEX2/AUR lysate assay time-course of 10 μM DADLE stimulation following siRNA transfection with HEK293 cells stably expressing UBC:DOR-APEX2. N=3 independent experiments were fit to a non-linear regression and analyzed with a two-way ANOVA (alpha=0.05, p=0.0233 for variation between siRNA treatments across the time-course, at 3 h p=0.0256 between siRNA treatments, all other timepoints=ns).

(e) Calculated $t_{1/2}$ for the rate of DOR trafficking to the lysosome in cells transfected with DNAJC13-targeting pool or siRNA control. Non-linear regression fit to data in 3D, N=3 independent experiments, were analyzed with a two-tailed, paired t-test (p=0.0051). **(f,g)** DOR internalization (f) and recycling (g) 72 h after transfection with siRNA control or siRNA pool targeting DNAJC13. Cell surface DOR was probed with anti-FLAG immunoreactivity and measured with a Beckman Coulter Cytoflex S, N=3 independent experiments, and data were analyzed using a two-tailed paired t-test.

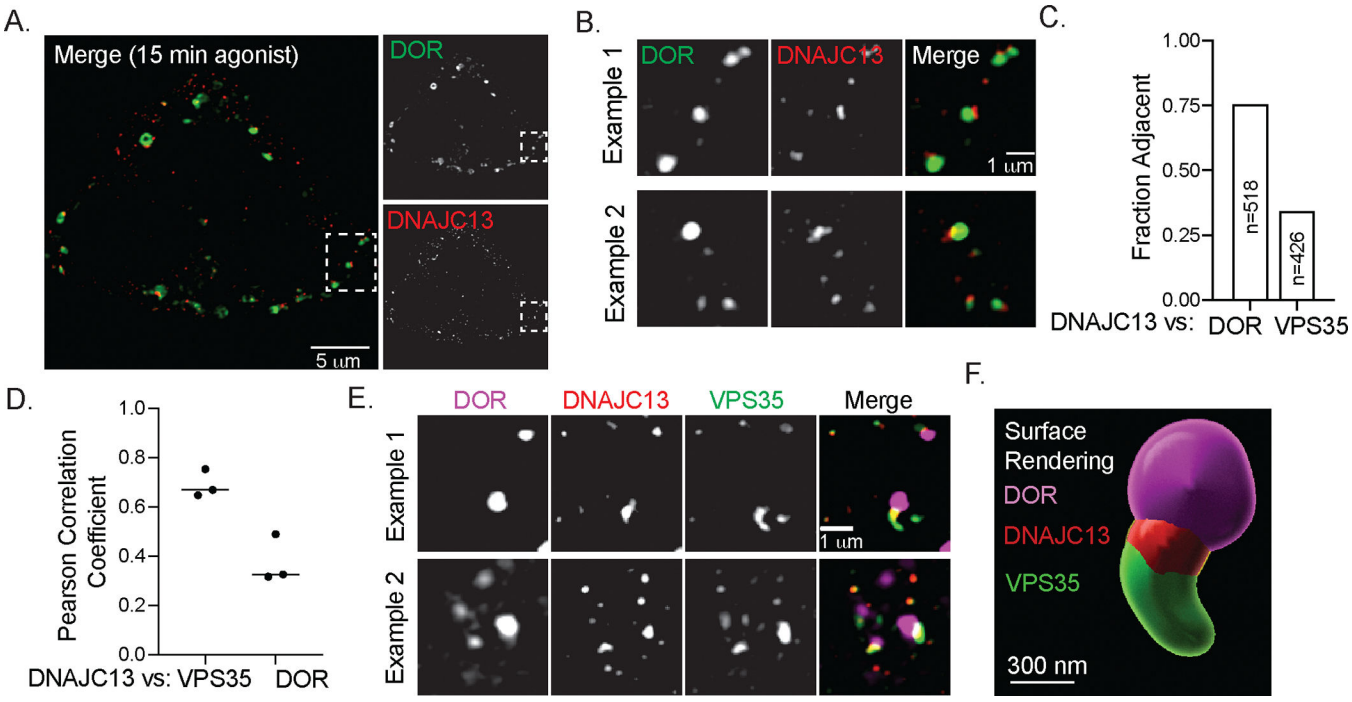

Figure 4: DNAJC13 localizes to DOR positive endosomes.

(a,b) Localization of DOR (anti-FLAG) and DNAJC13 (anti-DNAJC13) were analyzed in HEK293-FLP cells stably expressing UBC:DOR-APEX2 stimulated with 10 μM DADLE for 15 min. Image is single confocal slice, scale bar 5 μm in (a) and 1 μm (b). N=3 independent experiments, “Example 1” comes from white box in 4A, and “Example 2” comes from an independent replicate.

(**c**). Manual scoring of “adjacency” (i.e., <50% signal overlap of the DNAJC13 with either VPS35 or DOR when both signals appear on the same structure). N=3 independent experiments, total structures counted per condition noted.

(**d**) Pearson’s correlation coefficient calculated for DOR/DNAJC13 or VPS35/DNAJC13 from N=3 independent experiments, line denotes median.

(e) Localization of DOR (anti-FLAG), DNAJC13 (anti-DNAJC13), and VPS35 (anti-VPS35) were analyzed in HEK293-FLP cells stably expressing UBC:DOR-APEX2 stimulated with 10 μM DADLE for 15 min. Image is single confocal slice, scale bar 1 μm. N=3 independent experiments, “Example 1” comes from white box in Extended Data 6E, and “Example 2” comes from an independent replicate.

(h) Imaris software rendering of the surface of a single endosome from the Z-stack images from (4E) “Example 1”. Scale bar is 300 nm.

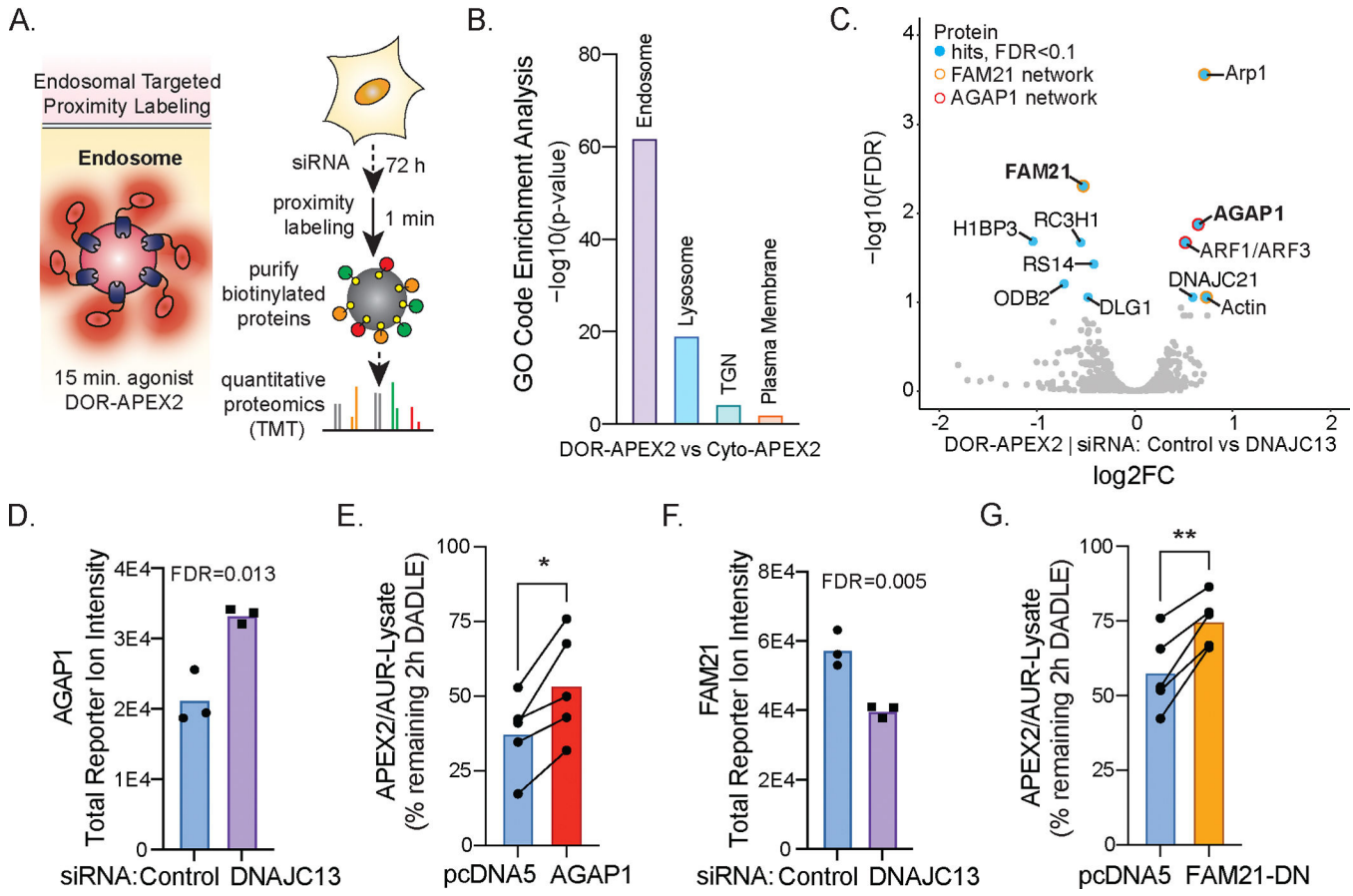

Figure 5: Loss of DNAJC13 remodels the endosomal DOR proteome.

(a) Endosome-targeted proximity labeling using DOR-APEX2.

(b) Gene ontology overrepresentation test comparing top 101 proteins (filtered by $\log_2$FC>1 and $\log_{10}$FDR<0.1) most enriched in DOR-APEX2 proximity labeling compared to cytoplasmic APEX2 control (CYTO-APEX2). Top 101 hits were analyzed using PANTHER analysis for “Slim Cellular Component” with a Fisher’s exact test with Bonferroni correction for multiple comparisons, and data plotted based on calculated p-value. Initial proteomic comparison of DOR-APEX2 vs CYTO-APEX2 (see Supplementary Table 3) from N=3 independent experiments were analyzed using edgeR’s exact test with Benjamini-Hochberg correction for multiple comparisons.

(c) Volcano plot of fold change (FC) comparing abundance of proteins following DOR-APEX2 mediated proximity labeling in cells transfected with siRNA control or siRNA pool targeting DNAJC13. N=3 independent experiments were analyzed using edgeR’s exact test with Benjamini-Hochberg correction for multiple comparisons. Proteins with an FDR <0.1 are denoted as hits (blue), hits linked to endosomal WASH/actin are highlighted with orange circles, and hits endosomal Arf/ArfGAP are highlighted with red circles. CCDC85C and DNAJC13 are outside the axis-limits of this plot and not displayed (see Supplementary Table 4)

(d,f) Total reporter ion intensity from TMT mass spectrometry from DOR-APEX2 proximity labeling in control cells or cells with DNAJC13 knockdown. N=3 independent experiments

were analyzed using edgeR's exact test with Benjamini-Hochberg correction for multiple comparisons, control vs DNAJC13 (AGAP1: FDR= 0.013; FAM21: FDR=0.005). (**e,g**) Effects of overexpression of AGAP1 or dominant negative FAM21 analyzed by the APEX2/AUR-lysate assay. Cells had no DADLE treatment or 2 h stimulation with 10 μM DADLE. N=5 replicates connected by lines and analyzed compared to empty vector using a two-tailed, paired t-test (AGAP1: p=0.0138; FAM21-DN: p=0.0039).

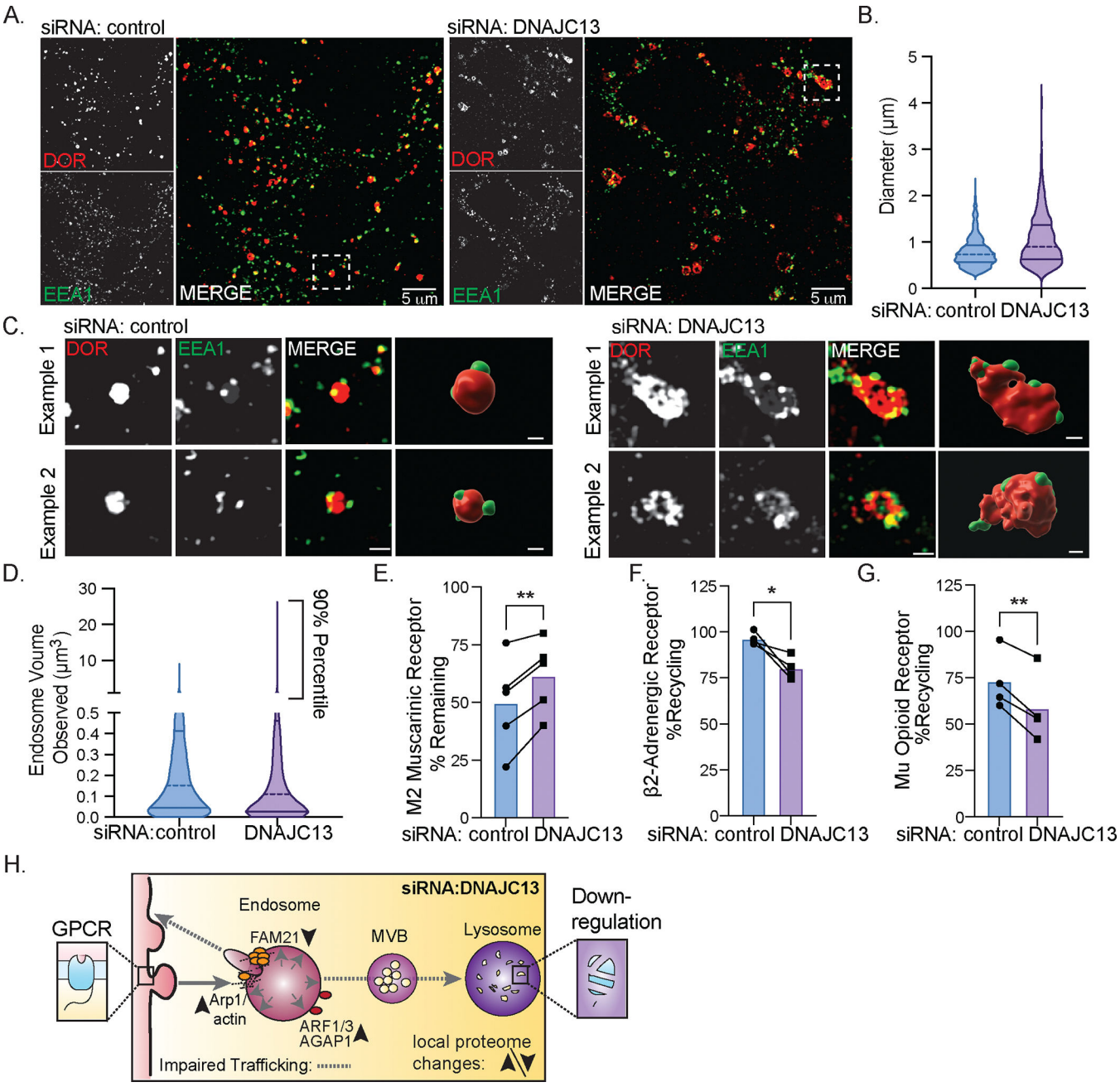

Figure 6: DNAJC13 knockdown causes expansion of DOR endosomes.

(**a,c**) Fixed and permeabilized HEK293-FLP cells stably expressing UBC:DOR-APEX2 were probed to detect endosomes (anti-EEA1) containing DOR (anti-APEX). Cells were treated with siRNA control or siRNA pool targeting DNAJC13 for 72 h prior to stimulated with 10 µM DADLE for 15 min. Image is single confocal slice, scale bar 5 µm in (a) and 1 µm in (c). N=3 independent experiments, “Example 1” comes from white box in 6A, and “Example 2” comes from an independent replicate. Scale bar for Imaris surface rendering is 500 nm.

(**b**) Diameter of DOR-and EEA1-positive endosomes was measured following knockdown of DNAJC13. N=3 independent experiments, control: 701 structures; siDNAJC13: 498 structures, median shown as dotted line and solid lines for the 25th and 75th quartiles.
(d) Volume of DOR- and EEA1-positive endosomes measured following knockdown of DNAJC13. N=3 independent experiments, control: 3714 structures; siDNAJC13: 3794 structures, median shown as dotted line and solid lines for the 25th and 75th quartiles.
(e) M2R trafficking to the lysosome analyzed 72 h after transfection with siRNA control or siRNA pool targeting DNAJC13 with the APEX2/AUR assay. Cells had no carbachol treatment or 4h stimulation with 10 μM carbachol. N=5 independent experiments were connected by lines and analyzed using a two-tailed paired t-test (p=0.0058).
(f,g) β2AR or MOR recycling 72 h after transfection with siRNA control or siRNA pool targeting DNAJC13. Cell surface DOR was probed with anti-FLAG immunoreactivity and measured with a Beckman Coulter Cytoflex S. N=4 independent experiments were connected by lines data and analyzed using a two-tailed paired t-test (β2AR: p=0.0337, MOR: p=0.0070).
(h) Working model describing the role of DNAJC13 in GPCR trafficking to lysosome and downregulation. Loss of DNAJC13 disrupts endosome homeostasis, a disrupted endosomal proteome with changed levels of key endosomal proteins, and impeded trafficking to the lysosome (downregulation) as well as the cell surface (recycling).